REJUVENATED VOLCANISM ALONG THE SOUTHWEST RIFT ZONE, EAST

MAUI, HAWAII: ERUPTIVE HISTORY OF THE HANA VOLCANICS

A THESIS SUBMITTED TO THE GRADUATE DIVISION OF THE UNIVERSITY
OF HAWAII IN PARTIAL FULFILLMENT OF THE
REQUIREMENTS FOR THE DEGREE OF

MASTER OF SCIENCE

IN

GEOLOGY AND GEOPHYSICS

MAY 1998

By

Eric C. Bergmanis

Thesis Committee:

John Sinton, Chairperson
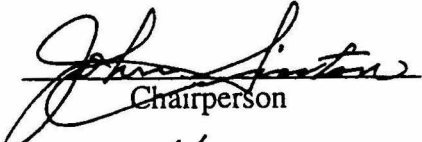Michael Garcia
Scott Rowland

We certify that we have read this thesis and that, in our opinion, it is

satisfactory in scope and quality as a thesis for the degree of Master of
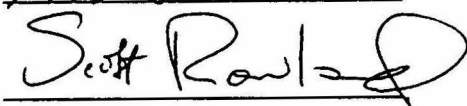
Science in Geology.

THESIS COMMITTEE

Chairperson

ACKNOWLEDGMENTS

TABLE OF CONTENTS

LIST OF TABLES

LIST OF FIGURES

INTRODUCTION

The evolution of Hawaiian volcanoes is marked by distinct growth stages (Macdonald and Katsura 1964; Clague and Dalrymple, 1987). The shield-building stage, which produces the bulk of the volume (90-95%) of the volcano, is typified by frequent eruptions of tholeiitic basalt. The post-shield stage forms a thin cap of alkalic lavas on most Hawaiian volcanoes with eruptive events occurring several hundred to several thousand years apart. The rejuvenation stage, one of the least understood facets of volcanism in the Hawaiian Islands, is marked by the onset of volcanic activity after periods of quiescence and erosion that last as long as 2.6 million years (Clague and Dalrymple, 1987). Lavas erupted during this stage are typically silica-undersaturated and range from alkalic basalts to nephelinites and melilitites. Rejuvenated volcanism does not occur on all Hawaiian volcanoes, and the processes controlling its inception, the nature of magma reservoirs and volcanism within this enigmatic stage are not clearly understood. Quiescent periods, number and frequency of eruptions, lava compositions, and spatial eruption distribution of rejuvenated volcanics vary from one volcano to another.

In this paper we describe the overall eruptive character of rejuvenated (Hana) volcanic activity on the southwest rift zone of the East Maui Volcano in order to gain an understanding of this stage of volcanism. A detailed lava flow map was made, lava chemistry and ^{14}C ages were determined to define temporal and spatial variations in eruptive frequency, erupted volumes, and lava chemistry. Crystallization simulations were run in order to gain some understanding of the conditions of magma evolution for this suite of lavas. Finally, the results of this study are used to assess potential volcanic hazards for southwest Maui.

1

Shield and post-shield stages of East Maui Volcano

East Maui Volcano is the younger and larger of the two volcanoes that make up the island of Maui (Stearns, 1940, 1946; Stearns and Macdonald, 1942). It is the only Hawaiian volcano other than those on the youngest island of Hawaii for which any quasi-historical record of volcanic activity exists, having last erupted ~1790 A.D. (Oostdam, 1965; Macdonald et al., 1983). Limited exposures of shield-building tholeiitic lavas, named the Honomanu Basalt, yield K-Ar ages of 1.10±0.05 Ma to 0.97±0.04 Ma (Chen et al., 1991). K-Ar ages of dated samples from alkalic post-shield Kula Volcanics overlying the Honomanu Basalt range from 0.93±0.33 Ma to 0.36±0.07 Ma (Chen et al., 1991; Naughton et al., 1980). Kula Volcanics are dominantly hawaiite with lesser amounts of alkalic olivine basalt, ankaramite, and mugearite and were erupted from three major volcanic lineations: the north, east, and southwest rift zones (Stearns and Macdonald, 1942; Macdonald and Katsura, 1964). The Kula Volcanics represent the longest lived and most voluminous post-shield stage yet documented in the Hawaiian Islands. Cessation of volcanic activity marked by the last of the Kula lavas ~360,000 yrs ago was followed by a period of quiescence long enough to develop large erosional features such as Kaupo valley, Keanae valley and Haleakala crater (Clague and Dalrymple, 1987). This quiescent period has important implications for estimates of erosional rates in the Hawaiian Islands as large features such as Keanae Valley, Kaupo Valley, and Haleakala Crater were cut into the East Maui Volcano during this time.

Hana Volcanics

Prior to this study the age of onset of rejuvenated volcanic activity on East Maui and hence the duration of the quiescent period between Kula and Hana activity was unknown. Clague and Dalrymple (1987) speculated that it might be as brief as 100-200 Ka. Hana Volcanics lavas are dominated by ankaramite and picrite, with lesser amounts of alkalic

2

basalt and hawaiite (Macdonald and Katsura, 1964). Of the three rift zones of East Maui Volcano, only the East (Hana) and Southwest rifts have been reactivated during rejuvenation volcanism.

The Hana Volcanics represent an unusual example of Hawaiian rejuvenation activity. The quiescent period separating it from the shield or post-shield stage is significantly shorter than for other rejuvenated volcanics in the Hawaiian Islands (Clague and Dalrymple, 1987). It is the only rejuvenation suite in the Hawaiian Islands whose spatial eruption distribution follows pre-existing rift zones developed during previous volcanic stages. Compared to the rejuvenation suites on Oahu, Kauai, and Niihau, Hana Volcanics lavas are generally less silica-undersaturated with no nephelinites or melilitites (Clague and Frey, 1982; Clague and Dalrymple, 1988). However, lava types similar to those of the Hana Volcanics are known from these rejuvenation volcanics as well as those from West Maui (Sinton et al., 1987) and East Molokai (Clague, et al. 1982). We will show in this paper that the total number of eruptions and eruption frequency also are greater for the Hana Volcanics than for rejuvenation suites elsewhere in the Hawaiian Islands.

Previous work on the Hana Volcanics

The mapping work of Stearns and Macdonald (1942) on East Maui concentrated primarily on distinguishing between the deposits of the shield, post-shield and rejuvenated volcanism, and within each series defining the areal extent covered by cinder cones, lava flows, and ash deposits. Brill (1975) investigated the southern flank of the lower southwest rift zone on East Maui from sea level to ~1650m and Horton (1977) studied the northern and southern flanks of the upper southwest rift zone axis from ~1650m to ~2930m. Their work produced the first lava flow maps and stratigraphic framework distinguishing the products of individual eruptive events of the Hana Volcanics for the southwest rift zone. They also documented vent and flow morphology as well as lithology

3

and petrography for individual eruptive units. The mapping in this study includes a synthesis, with some modifications, of the maps of Brill, Horton, and unpublished work by John Sinton. Macdonald (1978) produced a detailed geologic map of the Haleakala Crater area where he distinguished lava flows and pyroclastic deposits of Hana eruptions and defined stratigraphic relations between individual units.

Reber (1959) obtained the first ^{14}C dates for lavas of the southwest rift zone (Table 1). Crandell (1983) obtained several more ^{14}C dates for Hana lavas from both the east and southwest rift zones, estimated the ages of many others by extent of weathering, and produced the first assessment of volcanic hazards for East Maui volcano. To date, there is no absolute age data available for Hana lavas within Haleakala Crater.

The first compositional data for Hana lavas were obtained from rocks collected in Haleakala Crater (Macdonald and Powers, 1968; Macdonald, 1968). Previous geochemical investigations of East Maui lavas (including Hana) included samples from the east rift zone and Haleakala Crater (Chen and Frey, 1985; Chen et al., 1990; West and Leeman, 1987).

RESULTS

Mapping methods

The areal extent and stratigraphic relationships of the Hana Volcanics along the southwest rift zone (Figures 1, 2) were documented during eleven weeks of field mapping. The identification of individual eruptive units in the field was made primarily on the basis of lithological variations between lava flows; many units are lithologically distinct and easily recognizable in the field. Vertical, black and white aerial photos, Thematic Mapper Simulator images, and SIR-C synthetic aperture radar images provided guidance for areas where ground-based observations were indeterminate or impossible. Stratigraphic relations were determined by superposition, where possible, and in other cases, by extent of

4

Figure 1. Lava flow map for southwest rift zone Hana Volcanics. Correlation of map units shown in Figure 2.

Figure 2. Stratigraphic correlation chart for southwest rift zone Hana Volcanics units.

weathering and degree of vegetation cover. Geologic units belonging to the Hana Volcanics have been given names with an "h" prefix followed by a three letter suffix describing its location (vent name, land division, etc.). Lavas and pyroclastics of the Kula Volcanics were not subdivided by individual eruptive units and are labeled ku (Kula undifferentiated) and kc (Kula cinder).

Hana and Kula distribution

The mapped distribution of Hana and Kula Volcanics on the southwest rift zone presented in this study is only slightly modified from that of Stearns and Macdonald (1942). No southwest rift zone Kula rocks have been dated and there presently is no unambiguous method of distinguishing all Hana from all Kula lavas on the basis of major and trace element chemistry. Although the major and trace element composition of Hana and Kula lavas overlap, Kula lavas are in general less silica-undersaturated and more evolved than Hana lavas. The most common rock type for Kula lavas is hawaiite, with lesser amounts of alkalic basalt, ankaramite, and mugearite. In contrast, Hana lavas are primarily ankaramites and alkalic basalts, with rare hawaiites. In this work we have separated the deposits of Hana and Kula volcanic activity primarily on the basis of weathering extent and soil cover observed in the field. Kula Volcanics on the southwest rift zone may be extensively weathered, with soil cover ranging from a few centimeters to more than a meter in thickness. In places Kula topography is incised with gullies up 35 meters deep, and rock outcrops are typically sparse or non-existent except in the bottoms of stream-cut gullies. In contrast, the Hana Volcanics typically have little or no soil cover, morphological features such as lava channels and levees have been little modified since emplacement, rock outcrops are plentiful, and stream-cut gullies are almost non-existent.

Hana geologic unit distribution, vents, and lava types

We have identified 52 lithologically and chemically discrete units within the Hana Volcanics of the southwest rift zone. Vent locations for 17 of these units are unknown. There are seven vent structures such as Keokea, Keekeehia, and Molokini that cannot reasonably be associated with any of the 17 "ventless units". Thus, we have evidence for a minimum of 59 separate Hana Volcanics eruptions from the southwest rift zone.

The southwest rift zone can be divided into upper and lower segments based on differences in the orientation of volcanic lineaments and vent distribution. Hana vents along the upper one-half of the rift zone (between the elevations of 1650-2870 m above sea level) form a sharply defined, linear array trending N 65° E over a length of ~8.8 km. Vents on the lower rift zone (between the elevations of 60-1650 m above sea level) form a less well-defined linear array trending N 51° E over a length of 10.7 km. Most of the vents of the upper rift zone lineation occur just to the south of the topographic crest and all but four of the 22 flows in this area have traveled down the southern flanks of the volcano. There is a much more even distribution of lava flows on both the northern and southern flanks of the lower rift zone. Twelve eruptions have occurred at distances greater than two kilometers from the main rift zone axis. Nine of these twelve off-axis vents are broadly distributed on the southern flank of the southwest rift zone, whereas the remaining three are located on the northern flank. Pyroclastic fall deposits are much more prevalent on the northern flank of the rift zone; many lava flows are separated by cinder layers ~0.5-1.5 m thick whereas flows on the southern flank have little or no pyroclastic cover. The uneven distribution of pyroclastic fall deposits is almost certainly due to the prevailing trade winds, which typically blow from east to west across the rift zone axis.

Vent structures on the southwest rift zone are comprised of three main types: cinder cones, spatter cones and ramparts, and lava ponds. Cinder cones are the most common vent type. They consist of unconsolidated or slightly indurated glassy, vesicular clasts that

vary greatly in size and shape. Lava bombs are commonly exposed on cinder cone slopes and within the interior of cinder cones where incised by erosion. The largest of these cinder cones is Kanahau, which rises ~200m in elevation above the surrounding topography and is ~1 km in diameter at the base. Spatter cones and ramparts, far less common than cinder cones, are best represented by the vents of the ~1790 A.D. eruption. They are composed of agglutinated lava fragments several centimeters to tens of centimeters across that deformed upon impact while still partially molten. Three vents, producing units hgta, hlll, and hhan at 1945m, 465m, and 760m elevation respectively, are interpreted as being lava ponds. Devoid of pyroclastic material, they are roughly circular structures with raised edges and a central depression.

Some 90% of the lava flows from the southwest rift zone can be classified as a'a or transitional to a'a; rough clinkery surfaces and lava channels are ubiquitous features of these lava flows. Only about 10% of lava flows are pahoehoe, although numerous small exposures of pahoehoe can be found in the transitional lavas, especially near vents. Lava tubes are rare in southwest rift zone Hana lavas; most are less than 1 km from the vent area, less than a few meters to tens of meters in length, and less than 2m in diameter. One tube, in unit hgta however, is large enough to walk in, was traced for ~300m and may extend considerably further. Much larger tubes are present in Hana lavas in Haleakala Crater.

Age constraints

^{14}C ages

We have obtained 11 ^{14}C ages of charcoals from beneath lava flows and within pyroclastic layers along the southwest rift zone (Table 1) to supplement the 10 charcoal ages from Reber (1959) and Crandell (1983). Six of the 21 dated charcoals were taken from pyroclastic layers that have not been correlated with specific vents or lava flows; the

9

Table 1. [14]C and calibrated ^{14}C ages for southwest rift zone Hana Volcanics.

Geologic Unit	[14]C Age (^{14}C yrs B.P.)	Error (yrs)	Calibrated Age[1] (cal yrs B.P.)
hmke	510	±60	520
hmke[2]	590	±120	550
hkhh[2]	650	±140	600
hgta	830	±60	730
hlaa	860	±60	740
hhan1[2]	890	±170	780
hhan2[3]	920	±70	790
hnae	2,180	±60	2,150
hgab	3,000	±60	3,190
hhab	3,070	±60	3,210
hkam1[3]	3,900	±60	4,350
hkam2[3]	4,070	±90	4,530
FAT-96-16	4,840	±60	5,590
hale	8,190	±60	9,130
FAT-96-21	8,600	±60	9,520
W4557[3]	8,650	±90	9,540
FAT-96-14	10,440	±60	12,350
Pyroclastic Layer[3]	22,500	±310	~26,000[4]
Pyroclastic Layer[3]	26,800	±340	~31,000[4]
Pyroclastic Layer[3]	38,000	±450	~42,000[4]
hu	45,000	±1800	~50,000[4]

[14]C charcoal analyses for this study performed by John Mcgeehin of USGS Geologic Division Climate History Program. [1]Ages calibrated to calendar yrs by CALIB 3.0.3 software (Stuiver and Reimer, 1993). [2]Ages reported by Reber (1959). [3]Ages reported by Crandell (1983). [4]Age estimated by extrapolating ^{14}C calibration curve (Stuiver and Braziunas, 1993)

remaining 15 ages date lava flows. Two individual eruptions have two ages each, yielding a total of 13 dated eruptive events.

[14]C ages are not necessarily "true" or calendar ages because changes in the intensity of the Earth's magnetic field, the activity of the sun, and in the carbon reservoirs of the Earth due to climatic variations have produced time-dependent variations in the production of atmospheric radiocarbon (deVries, 1958; Olsson, 1970). Thus, ^{14}C ages calculated assuming constant radiocarbon content in the Earth's atmosphere, may not reflect the true age of the sample. Variations in the radiocarbon content of the atmosphere can be determined by comparing reported ^{14}C ages with the results of dendrochronology (tree-ring counting), uranium/thorium measurements in corals, and varve chronology of glacial lake sediments. These data have been used to create calibration curves to correct ^{14}C ages (Stuiver and Quay, 1981; Stuiver and Pearson, 1993; Pearson and Stuiver, 1993; Pearson et al., 1993; Linick et al., 1986; Kromer and Becker, 1993; Bard et al., 1993).

In this study, ^{14}C ages of less than ~10,500 yrs. B.P. are corrected using CALIB 3.0.3 software (Stuiver and Reimer, 1993) and are reported in cal yrs B.P. (calendar years before present), where the present is taken to be 1950 A.D. (Table 1). Well-defined calibration curves extend back only to ~18,000 ^{14}C yrs B.P. Thermoluminescence dating of quartz from aboriginal fireplaces compared to ^{14}C ages from the same locations provide calibration points that extend the calibration curve, although supported only by five analyses, back to ~30,000 cal yrs B.P. (Bell, 1991). Taken together, the results of ^{14}C calibration studies suggest that atmospheric ^{14}C content over the last ~30,000 years has steadily decreased with many short-term perturbations (Stuiver and Braziunas, 1993). Extrapolating the ^{14}C calibration curve, we can estimate what the difference might be between ^{14}C ages and true ages for samples older than ~18,000 ^{14}C yrs B.P. It is important to note, however, that these are estimates only, and do not represent real

11

calibrated ages. Although there is some uncertainty in calibration curves, calibrated ^{14}C ages are closer to the true age of the sample than uncalibrated ^{14}C ages.

Calibrated ages for southwest rift zone eruptions range from 520 to 50,000 yrs B.P. (Table 1). The abundance of age data for the period between 0 and 5,000 yrs B.P. relative to older age periods (Figure 3) means that our understanding of the absolute timing and order of southwest rift zone Hana eruptions is much better for this 5,000 year period than for the first few tens of thousands of years of Hana volcanic activity.

ca. 1790 A.D. eruptive event

The commonly accepted ca. 1790 A.D. date for the most recent eruption on the southwest rift zone, the Kalua O Lapa event (hkol), is not derived from charcoal analysis, but is based on differences between the coastline maps made by members of early western expeditions to Hawaii commanded by La Pérouse and Vancouver (Oostdam, 1965). The map of La Pérouse, made during his visit to Maui in 1786, shows a broad, gently curving bay between Puu Olai cinder cone and Cape Hanamanioa, which was formed during an eruption ~780 cal yrs B.P. Vancouver's map dates from 1793 and shows a conspicuous peninsula between the two points. Oostdam (1965) concluded that the differences between the maps suggests that the Kalua O Lapa event took place between the visits of the two European explorers, hence the ca. 1790 eruption date. Although the 1786 map from La Pérouse's expedition is too crude to conclude with certainty that the Kalua o Lapa lava was not present at the time of their visit, it seems clear from Vancouver's map that this eruption occurred prior to their visit in 1793. Other estimates based on Hawaiian oral history suggest that the eruption occurred between 1750-1770 (Stearns and Macdonald, 1942). Taken together, the available evidence suggests that the most recent eruption on East Maui occurred some 205-250 years ago.

12
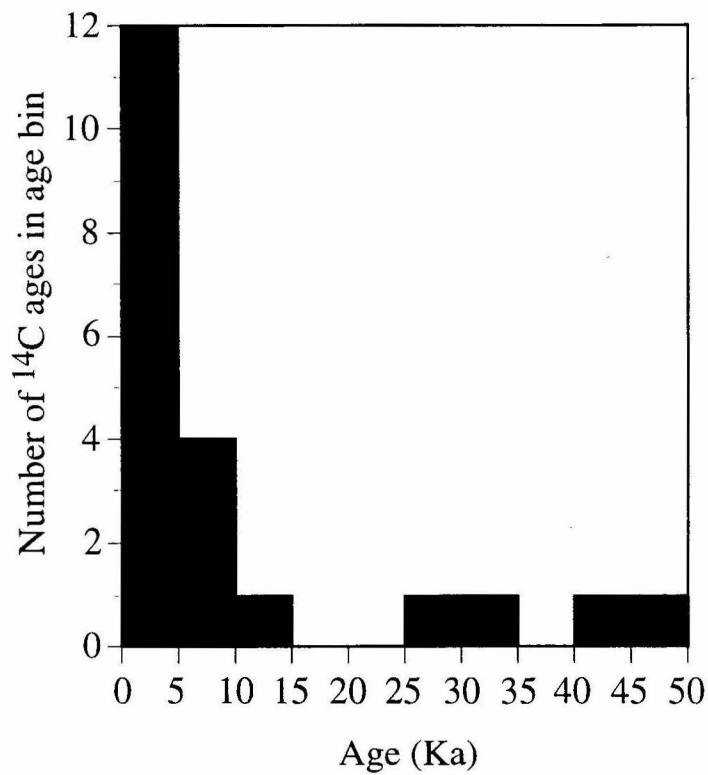
Figure 3. Histogram showing distribution of southwest rift zone ^{14}C ages. Dating is concentrated on the youngest units; we have the best understanding of eruption timing within the last 5,000 yrs.

Onset of Hana Volcanics

The oldest absolute age for a Hana eruption, a ^{14}C-derived date of ~50,000 years B.P. for a lava flow 2-3 km east of Kahua cone on the southern flank of the upper southwest rift zone, provides a minimum age for the onset of rejuvenated volcanism on the southwest rift zone. In an attempt to date four of the stratigraphically oldest Hana units for the area (hkha, hlll, hpaa, and hkah), rock samples were analyzed using the ^{40}Ar/^{39}Ar method. All of these samples showed evidence of excess Ar, and none yielded trustworthy ages (Pringle, pers. comm., 1997). Excess Ar is likely to produce an ^{40}Ar/^{39}Ar age that is older than the real age of the rock. The results obtained on one sample (hkha) indicated only that the age of the rock is less than 600 Ka. We can conclude that the other three analyzed units are younger than their ^{40}Ar/^{39}Ar ages plus two standard deviations (Table 2), giving maximum possible ages of units hlll, hpaa, and hkah of 60 Ka, 67 Ka, and 76 Ka, respectively. Although we do not know which Hana eruption is the oldest, we are confident that the 50,000 Ka ^{14}C dated lava and the three lavas dated with the ^{40}Ar/^{39}Ar method represent some of the oldest Hana eruptive activity on the southwest rift zone. Taken together, this evidence suggests an onset for Hana volcanism on the southwest rift zone of about 60,000 years ago ±15,000 years. This, however, does not preclude the possibility that rejuvenated volcanic activity elsewhere on East Maui began earlier than 60,000 yrs. ago. Since the youngest age for a post-shield Kula lava is ~360 Ka, the ~50,000 Ka minimum onset age for the Hana Volcanics implies that the period of quiescence between post-shield and rejuvenated volcanic activity on East Maui was no greater than ~310 Ka, the shortest yet documented on any Hawaiian volcano.

Table 2. $^{40}Ar/^{39}Ar$ ages and maximum possible ages for selected Hana lavas.

Geologic Unit	$^{40}Ar/^{39}Ar$ age (yrs)	Error, 1sigma (yrs)	Maximum age* (yrs)
hlll	58,000	1,000	60,000
hpaa	43,000	12,000	67,000
hkah	60,000	8,000	76,000

*Based on $^{40}Ar/^{39}Ar$ age plus 2 sigma.

Analyses performed by Malcolm Pringle III at Scottish Nuclear Reactor Center.

Petrography

Hand specimens of southwest rift zone Hana lavas show a wide range of lithologies, a trait that greatly simplifies the task of distinguishing the products of individual eruptions in the field. Within this petrographic variability, three broad groups can be defined based on phenocryst assemblages visible in hand sample.

Hana aphyric rocks are fine-grained, light gray to bluish in hand specimen, with rare (< 1%) olivine phenocrysts 1-4 mm in size. In thin section, there are an average of 4% olivine microphenocrysts smaller than 1 mm in a matrix of 10% groundmass olivine, 4% groundmass clinopyroxene, 45% plagioclase, 15% oxides, and 22% cryptocrystalline material not resolvable in thin section. Average groundmass grain size is approximately 0.4 mm. Most olivine microphenocrysts are euhedral or skeletal, but some are embayed. Plagioclase microphenocrysts mainly occur as tabular laths. Textures are typically trachytic, and the matrix may be cryptocrystalline to glassy.

Hana olivine-phyric rocks are typically dark gray in color with moderately abundant olivine phenocrysts 1-4 mm in size, and rare clinopyroxene phenocrysts that commonly are larger than the olivines. Thin section analysis reveals average modal percentages of 7% olivine phenocrysts, 15% groundmass olivine, <1% clinopyroxene phenocrysts, 11% groundmass pyroxene, 40% microphenocryst or groundmass plagioclase, 12%

15

groundmass oxides, and 14% cryptocrystalline or glassy material. Average groundmass grain size is 0.4 mm. Many olivine phenocrysts show embayed or skeletal outlines, yet euhedral outlines are moderately abundant. Clinopyroxene phenocrysts are typically subhedral or embayed. Groundmass clinopyroxenes are typically subhedral, interspersed with laths of plagioclase and oxide grains. Groundmass textures are typically felty or pilotaxitic; a few samples exhibit glassy textures.

Hana ankaramites are dark gray in color with abundant olivine and clinopyroxene phenocrysts in sub-equal proportions ranging in size from 1-10 mm. Modal percentages average 14% olivine phenocrysts, 10% groundmass olivine, 13% clinopyroxene phenocrysts, 8% groundmass clinopyroxene, 30% microphenocrysts of plagioclase, 12% groundmass oxides, and 13% microcrystalline material. Average groundmass grain size is 0.3 mm. Many olivine and pyroxene phenocrysts have embayed or resorbed outlines, yet euhedral and skeletal olivines also are common. A few samples contain rare plagioclase xenocrysts up to 20 mm in size with resorbed outlines. Clinopyroxene, interspersed with plagioclase laths and oxides, dominate the groundmass. Groundmass texture is typically felty; a few samples are glassy.

Chemical composition

One hundred rock samples from the ~250 collected by the authors were analyzed for major, minor and trace elements (Sc, V, Cr, Ni, Cu, Zn, Rb, Sr, Y, Zr, Nb, Ba, Th, and Pb) using a Siemens 303AS x-ray fluorescence (XRF) spectrometer at the University of Hawaii. Samples were broken with a tungsten-carbide plated hydraulic rock splitter, cleaned, and then crushed for approximately 1.5 minutes using a tungsten carbide mill. Loss on ignition was determined after samples were ignited for 8 hours at 900° C. Two fused buttons for major elements and one pressed powder pellet for trace elements were

16

prepared for each sample following procedures slightly modified from those of Norrish and Hutton (1969) and Chappell (1991). Each pressed powder pellet was analyzed twice.

Major and trace element data for selected southwest rift zone Hana Volcanics lavas are presented in Table 3. The 100 XRF chemical analyses of southwest rift Hana lavas that were obtained provide one or more analyses for 46 of 59 eruptive events documented.

Based on the classification schemes of Macdonald and Katsura (1964) and Le Bas et al. (1986), all of the lavas are alkalic and are mostly basanites with a few ankaramitic picro-basalts (Figure 4). CIPW norms were calculated for all of the analyzed samples; the total moles of iron for each sample were cast as 90% FeO and 10% Fe_2O_3. All of the samples are nepheline normative (3-17.5%). Samples from Haleakala Crater and the east rift zone also are all basanites and fall within the field formed by southwest rift zone Hana lavas. Although most Hana lavas from Haleakala Crater and the east rift zone have not been analyzed, the limited evidence available suggests that there is no systematic compositional difference in Hana lavas from different sections of East Maui.

MgO variation diagrams (Figure 5) reveal well-defined trends that are consistent with the lavas being related by varying degrees of fractional crystallization from a small range of parental melts. They span a wide range in SiO_2 (42.0-48.2 wt%) and MgO (3.3-13.6 wt%). Ankaramites have the highest MgO contents (>7.5 wt%). With decreasing MgO, contents of Al_2O_3, Na_2O, K_2O, and P_2O_5 increase (Figure 5). The steady increase in Al_2O_3 and P_2O_5 with decreasing MgO indicates that plagioclase and apatite were not fractionated from Hana magmas, consistent with thin section analyses which show that plagioclase and apatite phenocrysts are absent. At less than 8 wt% MgO, CaO contents decrease with decreasing MgO suggesting that Ca-rich clinopyroxene fractionated from magmas with less than 8 wt% MgO. With decreasing MgO below ~6.5 wt%, SiO_2 increases rapidly, and Fe_2O_3* and TiO_2 decrease, indicating that Fe-Ti oxides fractionated from Hana magmas with less than ~6.5 wt% MgO.

17

Table 3. Selected XRF analyses of Hana Volcanics lavas.

	EMH-56	EMH-34	EMH-31	EMH-52	EMH-1	EMH-28	BEM-63	EMH-86	BEM-71	BEM-44	EMH-65	EMH-18	BEM-163
Unit	hkhh	hpaa	hkai	hkam	hhab	hmah	hpim	hnae	hkno	hgta	hnin	hkol	hkeo
Rock Type	Aph	Aph	Aph	Aph	Ol	Ol	Ol	Ank	Ol	Ank	Ank	Ank	Ank
SiO_2	48.16	46.19	46.49	45.40	44.84	43.12	43.70	42.64	43.03	43.37	42.50	42.73	42.64
TiO_2	2.52	3.05	3.06	3.38	3.32	3.33	3.36	3.49	2.93	3.17	3.00	2.95	2.53
Al_2O_3	18.17	17.83	17.69	17.22	15.98	14.70	15.17	14.50	13.89	13.63	12.68	12.41	11.13
Fe_2O_3*	11.91	12.49	12.79	13.98	14.53	15.44	15.31	15.52	14.67	15.83	15.25	15.08	14.53
MnO	0.21	0.19	0.20	0.19	0.20	0.18	0.19	0.20	0.19	0.20	0.18	0.18	0.18
MgO	3.28	4.00	4.25	5.15	5.91	6.94	7.50	8.00	8.91	9.92	10.71	11.42	13.61
CaO	7.71	8.33	8.01	8.49	9.45	11.41	10.84	11.11	11.06	11.38	12.03	11.37	11.48
Na_2O	5.58	5.19	5.15	4.29	4.11	2.90	2.72	3.29	3.84	2.20	2.55	2.40	3.08
K_2O	0.20	1.89	1.90	1.62	1.68	1.05	1.19	1.02	1.12	1.00	0.83	0.87	0.72
P_2O_5	0.87	0.83	0.81	0.61	0.71	0.43	0.49	0.49	0.44	0.43	0.38	0.34	0.31
Total	98.61	99.99	100.36	100.34	100.74	99.50	100.47	100.26	100.07	101.11	100.11	99.76	100.21
LOI[a]	0.27	0.61	0.18	0.32	0.28	0.20	-0.50	-0.46	-0.27	-0.53	-0.47	0.16	-0.33
Sc	17	9	12	15	19	23	26	27	24	28	31	27	30
V	85	141	139	197	251	364	367	411	362	383	391	357	344
Cr	5	4	<2	5	55	138	187	199	387	379	529	549	758
Ni	<3	<3	6	6	43	84	83	80	154	128	183	277	312
Cu	36	12	25	29	94	77	58	45	68	46	53	112	69
Zn	124	116	118	102	119	108	113	115	111	117	108	103	101
Rb	53	45	46	38	42	27	29	27	28	24	21	22	17
Sr	1081	1155	1107	1035	962	678	750	755	649	617	595	532	496
Y	36	35	34	33	32	28	29	28	27	25	24	25	21
Zr	340	312	302	251	291	196	196	206	189	187	176	165	139
Nb	77	75	73	59	66	41	46	42	41	38	34	34	28
Ba	845	814	824	760	746	491	-	-	-	-	-	417	-

*Total iron is listed as Fe_2O_3

[a]LOI listed as total loss on ignition. Condition for ignition was 900°C for eight hours.

18
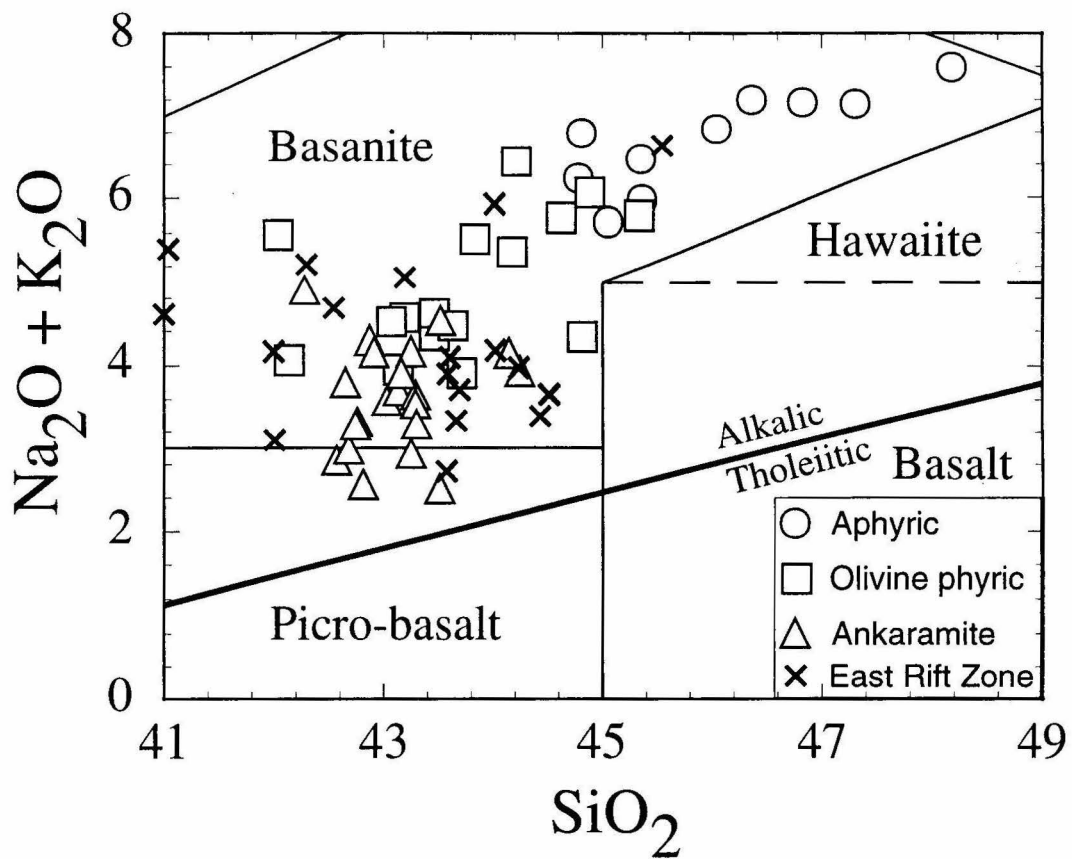
Figure 4.   Total alkalis versus SiO_2 (all in wt.%) for 46 southwest rift zone and 18
east rift zone Hana lavas (Macdonald and Powers, 1968; Chen et al.,
1990). Average compositions are shown where more than one analysis
exists for a single unit. All Hana lavas are alkalic (Macdonald and
Katsura, 1964). Adopting the classification from Le Bas et al. (1986), 41
Hana lavas are basanites, five are picro-basalts.
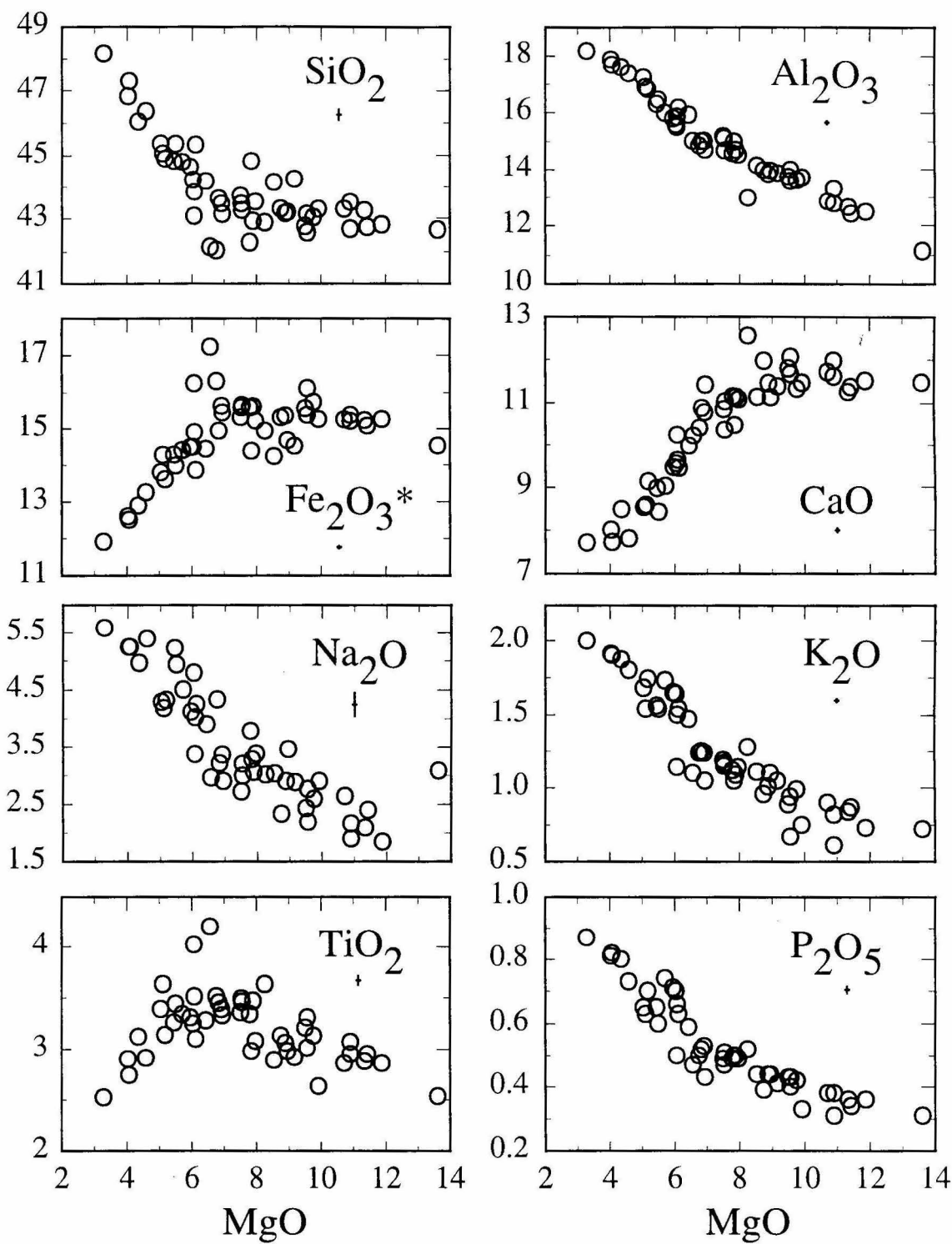
Figure 5. MgO variation diagrams of major element oxides (wt.%) for 46 southwest rift zone Hana lavas. Crosses indicate analytical uncertainties (2 sigma).

DISCUSSION

Conditions of magma evolution

Crystallization simulations were run using MELTS software (Ghiorso and Sack, 1995) in an attempt to reproduce major element trends consistent with this suite of Hana Volcanics lavas. The results are used to assess the likelihood of Hana lavas being related to similar parental melts by varying degrees of equilibrium or fractional crystallization and to determine the conditions at which these processes may have taken place. Sample EMH-49 (Table 3) was chosen as the parental liquid composition because its high MgO content reflects the least evolved magma on the main trend formed by the Hana lavas.

Major element variations indicate that Hana magmatic evolution occurred under conditions where plagioclase does not fractionate from magmas with more than ~3.5 wt% MgO. Experimental studies have shown that with increasing pressure, the liquidus fields of pyroxene and spinel expand at the expense of plagioclase. Similarly, with the addition of H_2O at constant pressure, olivine and pyroxene fields expand, suppressing the onset of plagioclase crystallization to lower temperatures and MgO contents (Yoder and Tilley, 1962; Nicholls and Ringwood, 1973; Bender et al., 1978). To explore the effects of varying pressure and H_2O contents on the crystallization path, simulations were run with pressures from 1 bar to 6 kbar and H_2O contents of 0.1, 0.5, 1.0, and 2.0 wt%.

The best results were achieved using 3 kbar pressure and 0.5 wt% H_2O (Figure 6). Using these parameters, the major element trends in the Hana lavas can be approximated using both equilibrium and fractional crystallization simulations. Under these conditions, olivine begins to crystallize at about 1300° C, clinopyroxene between 8-9 wt% MgO, and Fe-Ti oxides around 6 wt% MgO. Plagioclase does not begin to fractionate until MgO contents are below 4 wt%. Although increasing pressure and increasing H_2O content as independent variables tend to suppress the onset of plagioclase on the liquid line of descent,

21

Figure 6.   Results of MELTS simulations plotted along with Hana data (wt.%) on MgO variation diagrams. All simulations shown were run with 0.5 wt.% H_2O. Results of simulations suggest that Hana magmas undergo evolutionary processes at depths of ~10-11 km (3 kbar) suppressing the onset of plagioclase crystallization and fractionation until MgO content is below ~3.5 wt.%.

22

the simulations required the combined effect of moderate pressures and H_2O contents to best approximate major element trends observed in Hana lavas.
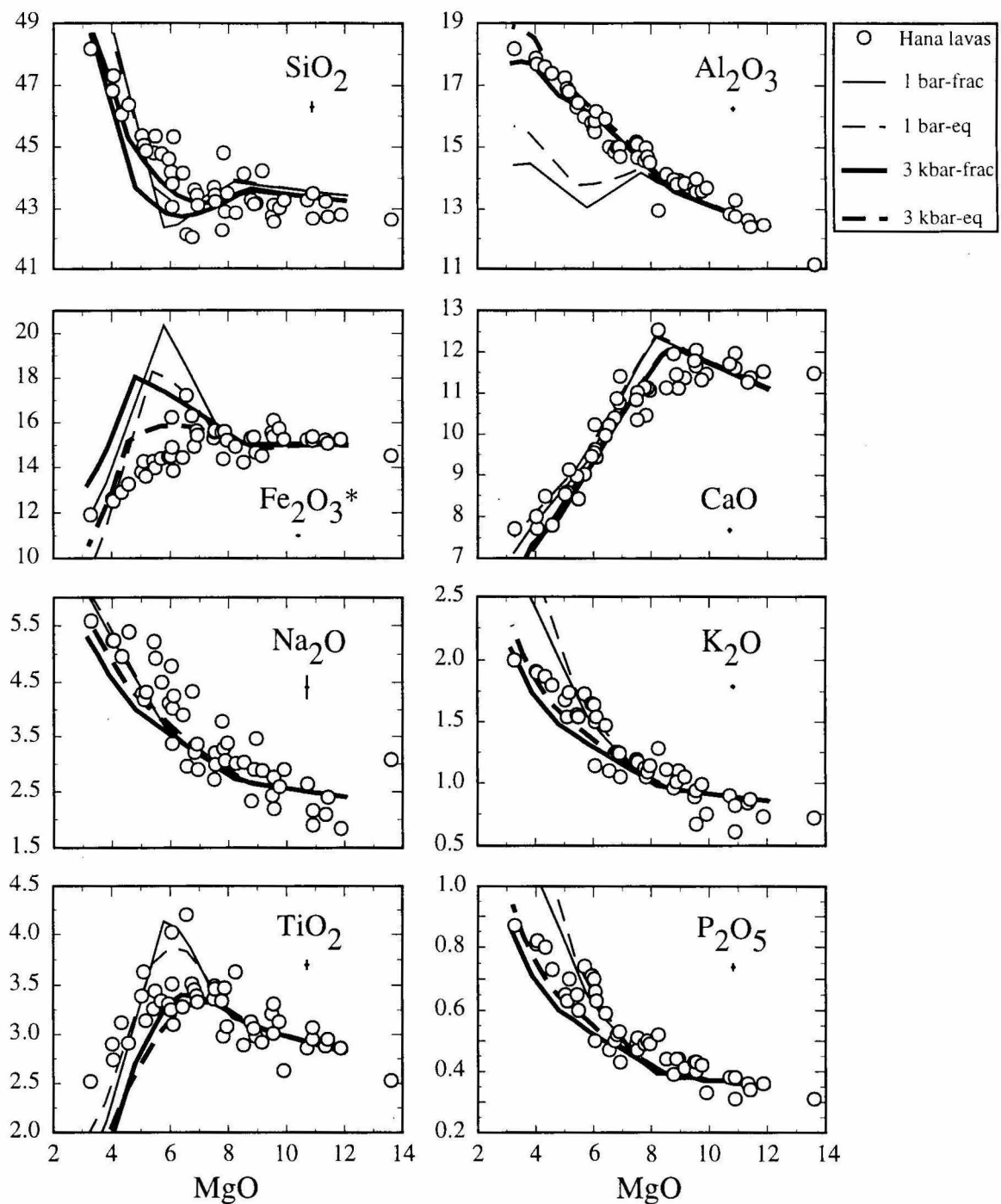
Simulations using 0.1 wt% H_2O required at least 6 kbar of pressure to suppress the onset of plagioclase to 3.5 wt% MgO, but produced model Al_2O_3 contents higher than the actual Hana lavas for a given MgO content. Additionally, these simulations produced trends for other major elements that were inconsistent with Hana data. Simulations using low pressures and variable H_2O contents were equally unsuccessful. For example, simulations using atmospheric pressure began crystallizing plagioclase around 8 wt% MgO regardless of H_2O content. Using slightly higher pressures of 0.5-1.0 kbar while varying H_2O from 1-2 wt% did suppress the onset of plagioclase to at least 3.5 wt% MgO, but the Al_2O_3 trend as well as those of the other major elements were inconsistent with those of Hana lavas.

Although the simulations imply that fractional crystallization may be the dominant process in the evolution of Hana lavas, comparisons between the major element trends of the simulations and the southwest rift zone sample data suggest that magma mixing may also play a role. The simulated Fe_2O_3* trends generally match those of the southwest rift zone samples at high and low MgO values (Figure 6). However, between ~8.0-4.5% wt% MgO, the Fe_2O_3* contents of the Hana lavas are significantly lower than those produced by the simulations. It is possible that the lavas between ~8.0-4.5 wt% MgO formed from the mixing of primitive and evolved magmas derived from similar parental magmas.

The results of the MELTS simulations are important as they suggest that Hana magmas are undergoing evolutionary processes at a pressure of ~3 kbar. If we assume an average crustal density of 2.9 gm/cm^3 , this yields a depth of ~10-11 km. Although southwest rift zone Hana lavas show a wide range of chemical compositions, they appear to be derived from a small range of parental magma compositions and are related by varying degrees of fractional crystallization. A small, intermittently tapped and

23

replenished, deep crustal magma reservoir is consistent with these observations. It also accounts for the absence of high-pressure xenoliths that are found in some rejuvenation suites elsewhere in Hawaii because xenoliths would likely be segregated from the magma while it resided in the magma chamber (Clague, 1987). Chen et al. (1990) suggested that Kula geochemical data are consistent with evolutionary processes occurring in a fairly shallow-level magma chamber, including significant fractionation of plagioclase feldspar. The Hana lavas examined here are consistent with evolution at a depth that suppresses the onset of plagioclase, implying that the magma reservoir present during the evolution of rejuvenated Hana lavas is significantly deeper than the one present during the post-shield stage.

The crustal model of Moore (1987) suggests that the boundary between the base of the volcanic edifice of East Maui and the top of the older oceanic crust is ~13 km deep and the boundary between the base of the oceanic crust and the upper mantle is at a depth of ~19 km. A magma reservoir 10-11 km deep would be just above the base of the volcanic edifice. Petrologic investigations of magmas and xenoliths from other rejuvenated suites in Hawaii and Hualalai Volcano (post-shield stage) suggest that magmas are rising rapidly from depths of 20 km or more, below the crust-mantle boundary (Moore et al., 1987; Clague and Dalrymple, 1987). Small volume, infrequent eruptions of lava containing mantle xenoliths imply that there is no crustal magma chamber present underneath Hawaiian volcanoes producing these lavas. The lack of mantle xenoliths and the results of MELTS simulations suggesting the presence of a deep-crustal magma reservoir imply that magma reservoir processes associated with rejuvenated volcanism on East Maui is significantly different than for other Hawaiian rejuvenation suites.

24

Co-eruptive sequences

An important facet in reconstructing the eruptive history of the southwest rift zone has been the recognition of several multi-flow sequences which may have been part of a single eruptive event (Figure 7). These co-eruptive sequences are important in defining the eruptive character or style of rejuvenation stage volcanic activity on the southwest rift zone. Here we have evidence that co-eruptive activity, long suspected in areas like the Koko Rift within the Honolulu Volcanics, is a part of rejuvenation stage activity in the Hawaiian Islands. As one of the main goals of this research is to define eruption frequency within the Hana Volcanics, the recognition of co-eruptive sequences is important as it reduces the total number of eruptive events that have taken place on the southwest rift zone by combining as many as four vents and flows into one eruptive event. The presence of co-eruptive sequences also has a direct effect on our estimates of volumes erupted during an individual event with consequent implications for volcanic hazard assessment. The two geologic units with the greatest estimated volumes (hkam, hmak) are examples of co-eruptive sequences.

Perhaps the best example of a co-eruptive sequence is the Hanamanioa sequence, with four members (hhan, Fig. 7). The lavas are essentially identical chemically (Table 4), all are moderately olivine phyric, almost indistinguishable in hand sample; two of the members have been dated at ~780 cal yrs B.P., and the vents from which the lavas were erupted fall on a straight line. Taken together, these data strongly suggest that these four flows erupted from discrete vents are the products of a single eruptive event from a fissure ~3.3 km long.

It is important to note that the correlation of individual members of a co-eruptive sequence are not made on the basis of similar chemical composition and petrography alone. Lavas erupted in unrelated events, but derived from similar parental melts and conditions of magmatic evolution should have very similar chemical compositions. Although the lavas
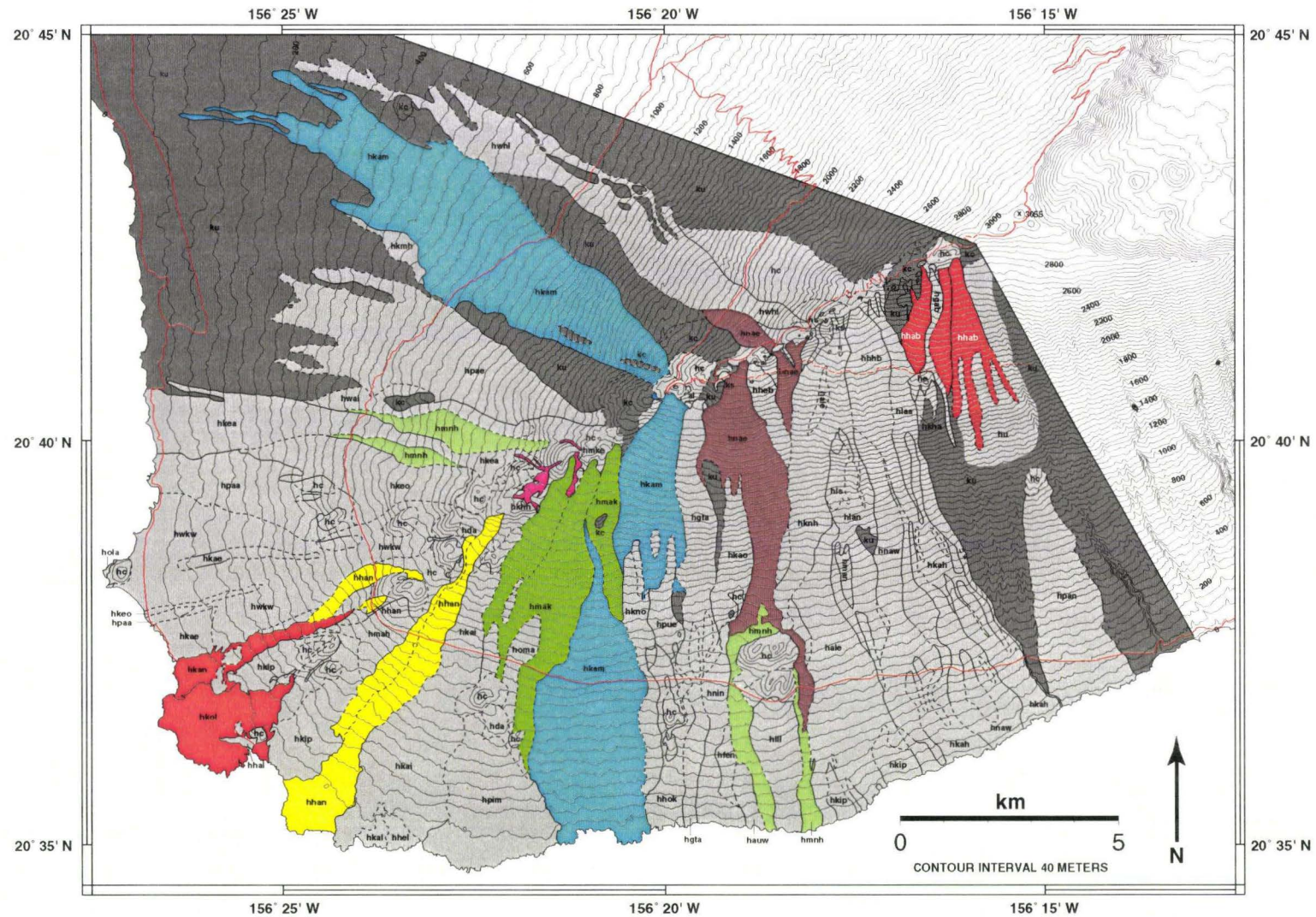
25

Figure 7. Map showing distribution of eight southwest rift zone co-eruptive sequences. Individual members of each sequence are shown in the same color. Hanamanioa sequence discussed in text is shown in yellow.

within six of the co-eruptive sequences identified in this study are compositionally very similar, we have not assumed that the products of individual eruptions must necessarily be chemically uniform. There are two other examples in the area, where spatial and age information supports the interpretation that they are co-eruptive, but where the individual lava flows are compositionally distinct. The lava flows of units hmke and hkhh are only about 0.5 km apart and appear to emanate from a single continuous fissure that cuts across Puu Makua, a cinder cone formed in a previous eruption. Independent ^{14}C ages show that hmke was erupted ~550 ±120 cal yrs B.P. and hkhh was erupted ~600 ±140 cal yrs B.P.; analytical error of these ages indicates that the two events may have occurred essentially simultaneously. However, the chemical compositions of the two lava flows are extremely different, with MgO values between the two varying by ~6.0 wt. %. Another example of a possible co-eruptive sequence is the ca. 1790 A.D. flow (hkol), and hkan, which was erupted ~2 km uprift of hkol. The two spatter rampart vent structures form a co-linear array, and they appear to be of similar age, although stratigraphic relations of their contact show that hkol is (slightly?) younger than hkan. It is not clear if the quasi-historical accounts of the 1790 A.D. eruption refers to both flows. These two flows are compositionally distinct from one another, differing by ~3 wt% MgO. Thus, in these two examples, separate, but spatially associated lava flows close in age have different chemical compositions. In summary, we have confidently identified six co-eruptive sequences along the southwest rift zone that are chemically identical and two other examples where the relationships are less clear.

Total number of Hana eruptions

On the axis and flanks of the southwest rift zone, the Hana Volcanics appear to form a very thin veneer of lavas, in most places probably only 1-3 flows thick, lying on top of the Kula Volcanics. This is based primarily on our ability to differentiate between Hana and Kula

27

Table 4. Age and chemical composition for individual
members of the Hanamanioa co-eruptive sequence.

	EMH-26	EMH-27	EMH-29	EMH-30
Rock Type	Ank	Ank	Ank	Ank
Age[1]	780	780	-	-
SiO_2	42.60	42.85	43.06	42.93
TiO_2	3.60	3.61	3.67	3.65
Al_2O3	12.84	13.00	13.08	13.03
Fe_2O_3*	14.87	14.91	15.06	14.93
MnO	0.20	0.19	0.19	0.19
MgO	8.15	8.04	8.34	8.28
CaO	12.48	12.50	12.41	12.59
Na_2O	3.05	3.26	3.06	3.31
K_2O	1.25	1.28	1.28	1.30
P_2O_5	0.51	0.53	0.52	0.52
Total	99.56	100.17	100.68	100.73
H_2O	0.20	0.11	0.19	0.14
CO_2	0.16	0.12	0.14	0.03
Sc	31	31	27	28
V	406	406	380	389
Cr	305	283	196	277
Ni	135	129	119	133
Cu	166	173	129	122
Zn	111	110	109	110
Rb	29	29	30	29
Sr	762	770	758	761
Y	26	27	27	26
Zr	232	234	237	233
Nb	49	50	50	50
Ba	528	519	521	505

[1] cal yrs B.P.
* Total iron is listed as Fe_2O_3

lavas on the basis of soil cover and extent of weathering observed in the field. The northern flank of the central and upper southwest rift zone is only partially covered by Hana lava and cinder widely separated by large kipukas of weathered Kula lavas. Despite the fact that Hana lava flows have preferentially traveled down the southern flank of the southwest rift zone, there are still several widely distributed kipukas of older Kula lavas present. It seems reasonable that only a fairly thin veneer of young lavas would allow for the presence of such large and broadly distributed kipukas of older terrain. Although the northern flank of the lower rift zone has been completely covered by Hana lavas, much of this lava appears quite old and may represent some of the earliest rejuvenated volcanic activity on the southwest rift zone. Only on the southern flank of the lower rift zone, where the area has been completely covered by Hana lavas and volcanic activity has continued into the last millennia, is the section of rejuvenated lavas likely to comprise more than three or four separate lava flows. Thus, we feel that there cannot be many additional Hana lavas hidden under the mapped units, and that the 59 identified units probably represent the great majority of the rejuvenated volcanic activity that has taken place along the southwest rift zone (Figure 1).

The total number of Hana eruptions that have taken place on East Maui is not known. Some of the lavas shown on the map of Haleakala Crater (Macdonald, 1978) are not separated as to source, and no lava flow map for the east rift zone outside of Haleakala Crater exists. However, a simple count of vents using the map of Haleakala Crater and aerial photographs of the east rift zone reveal roughly the same concentration of vents per unit length of rift zone. Stearns and Macdonald (1942) suggested that the section of Hana Volcanics on the east rift zone might be somewhat thicker than on the southwest rift zone based on the lack of kipukas of older Kula lavas. It is plausible that there may have been about as many Hana eruptions per unit length of rift zone in the crater and along the east rift zone as along the southwest rift zone. Since 59 eruptions have occurred along ~40% of the

29

subaerial rift zone of East Maui, we can estimate that there may have been an additional 80 to 90 eruptions along the east rift zone including the portion within Haleakala Crater. The estimated total of 140-150 Hana Volcanics eruptions is at least three times greater than the total number of eruptions for each of the Honolulu and Koloa Volcanics rejuvenation suites on Koolau and Kauai Volcanoes (Lanphere and Dalrymple, 1980; Clague and Dalrymple, 1988).

Eruption frequency

Estimates of eruption frequency along the southwest rift zone are based on our understanding of the age of onset of the Hana Volcanics, the total number of Hana eruptive events that have taken place, ^{14}C dates for individual lava flows, and stratigraphic relationships of lava flows surrounding the dated units.

A least 59 eruptive events have occurred in ~60,000 years; this yields an average eruption frequency of ~1/1017 years for the entire duration of rejuvenated volcanic activity along the southwest rift zone. However, ^{14}C dates and stratigraphic relationships show that, of these 59 eruptions, at least 13 were erupted in the last ~4,400 years, and of these, six were erupted between ~780 and 180 cal yrs B.P. Thus, eruption frequency apparently has progressively increased from 1/1200 yrs (~60,000-4,400 yrs ago) to 1/520 yrs (4,400-780 cal yrs B.P.) to 1/100 yrs (~780-180 cal yrs B.P.) (Figure 8). Although the southwest rift zone erupted, on average, every 100 years between 780-180 cal yrs B.P., it has not erupted since. This result suggests that the southwest rift zone is statistically overdue for an eruption.

Our understanding of the absolute ages and order in which eruptions have occurred on the southwest rift zone is understandably much greater for the period covering the last few thousand years than it is for the first few tens of thousands of years of rejuvenated volcanic activity. We are confident that we have documented and at least approximated the
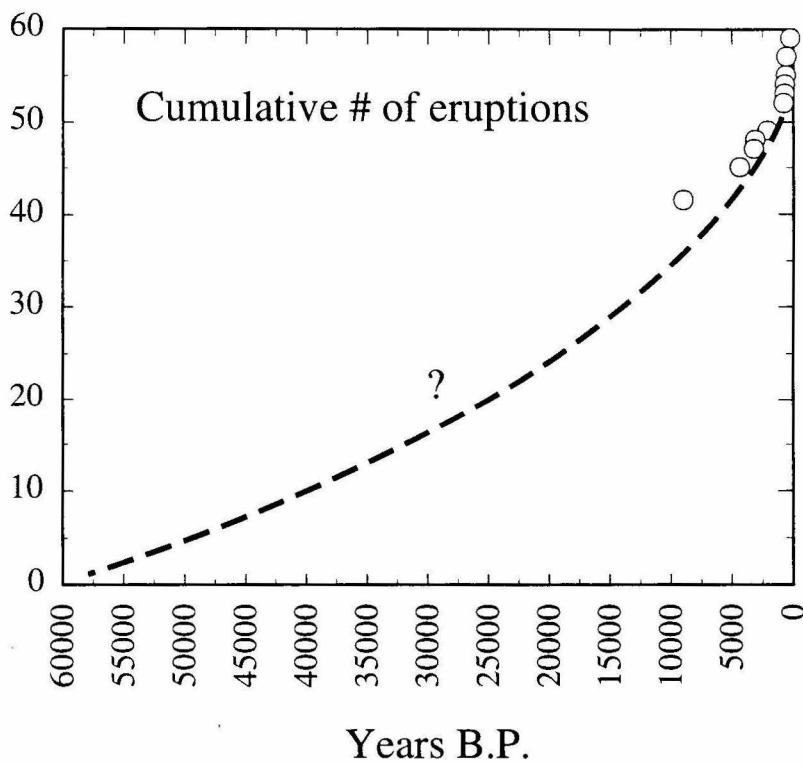
30

Figure 8.   Cumulative number of eruptions versus time for southwest
rift zone eruptive events. 13 of 59 eruptions have taken place
in the last 4400 years. It is not known if eruption frequency
increased steadily throughout the duration of Hana activity.

ages of all the eruptive events that have taken place since ~780 cal yrs B.P. Thus, until the next eruption occurs from the southwest rift zone, our estimate of eruption frequency during this period (~1/140 yrs, ~780 cal yrs B.P.-present) will not change. However, as many as five additional eruptive events may be added to the age group ~4,400-780 cal yrs B.P. These five lavas appear similar in age to nearby lavas that have been shown to be equal to, or younger than, ~4,400 yrs, and the local stratigraphy does not prohibit their placement in that age group. Even if the number of eruptive events in the age group ~4,400-780 cal yrs B.P. grows from seven to twelve, the adjusted eruptive frequency for this age group (~1/302 yrs.) will still be considerably less than for the group less than 780 cal yrs B.P. In fact, the removal of those seven eruptive events from the older age group (>4,400 yrs) would decrease its eruptive frequency, resulting in an even greater increase in eruptive activity in the last ~4,400 yrs. Since we are confident that rejuvenated volcanism along the southwest rift zone began at least ~50,000 yrs. ago, this trend of eruptions becoming more frequent towards the present could be offset only if we have not documented ~100 eruptive events that have occurred in the first ~46,000 yrs of Hana volcanic activity. In view of the field evidence for only a relatively thin veneer of Hana lavas in the area, we consider this possibility to be highly unlikely.

It is important to recognize that our estimates of eruption frequency are for the southwest rift zone alone. Reliable estimates of eruption frequency for the entire Hana Volcanics are not possible because it is not clear how many Hana eruptions have taken place along the east rift zone and only three ^{14}C ages for Hana eruptions outside of the southwest rift zone exist (490, 9400, and 12,760 yrs B.P.; Crandell, 1983). These data show that there has been at least one eruption in the last 500 yrs outside of the southwest rift zone, and that dated volcanic activity on the east rift zone falls within in the same period known for the southwest rift zone. If Hana volcanic eruptions along the east rift zone have occurred with similar frequency as on the southwest rift zone, our estimate of the average

32

frequency of eruptions for East Maui would be doubled, ~1/500 yrs for the entire span of rejuvenated activity. This estimated eruption frequency is roughly two orders of magnitude greater than estimates of eruption frequency for the Honolulu and Koloa rejuvenation suites on the Koolau and Kauai Volcanoes (Lanphere and Dalrymple, 1980; Clague and Dalrymple, 1988)

Local recurrence rates

Kipukas of post-shield Kula lavas show that some areas on the axis and flanks of the southwest rift zone have not been resurfaced by the products of rejuvenation stage Hana lavas. Within the Hana Volcanics, the frequency with which volcanic activity recurs locally varies dramatically along the axis and flanks of the southwest rift zone. Statistically meaningful estimates of eruption frequency and intervals between coverage by lava flows for specific areas along the southwest rift zone are impossible because of the small number of eruptions that have taken place in localized areas and the lack of accurate ages for older Hana eruptive events. However, based on our understanding of overall eruption frequency and areal distribution of lava flows, we can say that the smallest recurrence intervals (several hundred to at least seven thousand years) occur on the rift zone axis and higher elevations of the south flank of the southwest rift zone. Most eruptive events originate on the rift zone axis, a significantly higher proportion of lava flows travel down the south rather than north flank, and small volume eruptions at the rift zone axis are more likely to cover areas at higher elevations. Recurrence intervals for the north flank and lower elevations of the south flank are probably much greater (~7000->10,000 yrs.?) because fewer eruptions originate in this area and only lavas from relatively high volume eruptions are likely to reach lower elevations.

Lava flow areas and volumes

Reliable estimates of lava flow areas are limited to those geologic units where there is complete or near complete subaerial exposure. Thus, the 21 eruptive events for which we have estimated area and volume are those that lie at or near the top of local stratigraphy. Subaerial lava flow lengths range from 0.5 to 13 km and widths range from a few tens of meters to as much as 3 km. Lava flows from 44 of the 59 documented eruptive units have reached elevations of 400 m or lower and at least 28 have reached the ocean. Where flows have entered the ocean, areas and volumes are given as minima based on subaerial exposures. Accurate estimates of lava flow thickness are hampered by a lack of knowledge of pre-eruption topography. Most estimates of lava flow thickness were made at flow margins, but the edges of kipuka and rare erosional gullies provide a few opportunities for thickness measurements in the central parts of flows. The calculation of lava flow volumes is dominated by flow areas. Despite the uncertainties, we feel that our thickness estimates probably are within a factor of two. Thus, our lava flow volume estimates probably do not vary from the true volume by more than a factor of two. Volume estimates are probably most accurate for thin, small area flows where the ratio of exposed margin to flow area is large, and least accurate for thick, large area flows. The total volume of Hana lavas erupted from the southwest rift zone (~2.42 km^3) is estimated by calculating the total subaerial exposure of Hana lavas and multiplying by an estimated average thickness of 10 meters. Clearly we believe that the Hana Volcanics from the southwest rift zone form only a very thin veneer of lavas lying on top of the post-shield Kula Volcanics. Calculated individual unit areas range from 0.14 km^2 ->40.44 km^2 and volumes from 0.0003 to >0.40 km^3 (Table 5).

Although the volume of lava produced by individual eruptive events may vary as much as three orders of magnitude, the overall production of lava per unit time is dominated by eruptive frequency. Numerous small volume eruptions closely spaced in

34

time may produce as much lava as one or two widely spaced, large volume eruptions. Thus, while there certainly have been fluctuations in lava volume produced throughout the time interval spanning the Hana Volcanics, the increase in eruption frequency discussed earlier has led to an overall increase in total lava production per unit time (Figure 9). In fact, ~1 km^3, or roughly 40% of the total volume of Hana Volcanics from the southwest rift zone has been erupted in the last ~5000 years, or less than ~10% of our estimated total duration for southwest rift zone Hana activity.

Temporal variation in lava composition

Limited age data on the older eruptive events along the southwest rift zone precludes a complete assessment of temporal variation in composition of Hana lavas throughout the entire span of rejuvenated volcanic activity. However, the record of eruptive events occurring from ~4400-180 cal yrs B.P. is almost complete. Of the 19 events placed within this time interval, ages for 11 are constrained by ^{14}C or quasi-historical reference, 4 are constrained by stratigraphic relationships with ^{14}C-dated units, and 4 age estimates are based on extent of weathering and vegetative cover in close proximity to ^{14}C-dated units.

Plots of major and trace element contents versus time for these 19 eruptive events show that, with the notable exception of unit hkhh erupted ~600 cal yrs B.P., the most evolved lavas were erupted some 3,000-4,500 cal yrs B.P. (Figure 10). Since that time, lavas erupted from the southwest rift zone have been primarily less evolved ankaramites and alkalic olivine basalts.

There is limited evidence that there may be discrete pulses or episodes of volcanic activity on the southwest rift zone, separated by periods of relative inactivity. When the compositional data for the last ~4,500 yrs. (Figure 10) is compared to a lava flow age map (Figure 11), it shows that the more evolved lavas erupted ~3,000-4,500 cal yrs B.P. were

35

Table 5. Areas, average thicknesses, and estimated volumes for selected southwest rift zone lava flows.

| Unit	Area (km^2)	Thickness (meters)	Volume (km^3)
hmke	0.14	2	0.0003
hkha	0.21	3	0.0006
hkhh	0.35	2	0.0007
hgab	0.60	4	0.0024
hkan	1.96	4	0.0078
hkaa	2.69	4	0.0107
hkol	4.09	3	0.0123
hhab	4.64	5	0.0232
hpim	6.29	4	0.0252
hgta	5.32	5	0.0266
hkea	7.04	4	0.0282
hhhb	5.66	5	0.0283
hhan	7.64	3	0.0296
hknh	5.63	6	0.0338
hnae	8.35	5	0.0377
hpae	11.55	4	0.0462
hpan	6.67	7	0.0467
hwhl	9.90	5	0.0495
hkai	13.87	6	0.0832
hmak	16.18	8	0.1294
hkam	40.44	10	0.4044
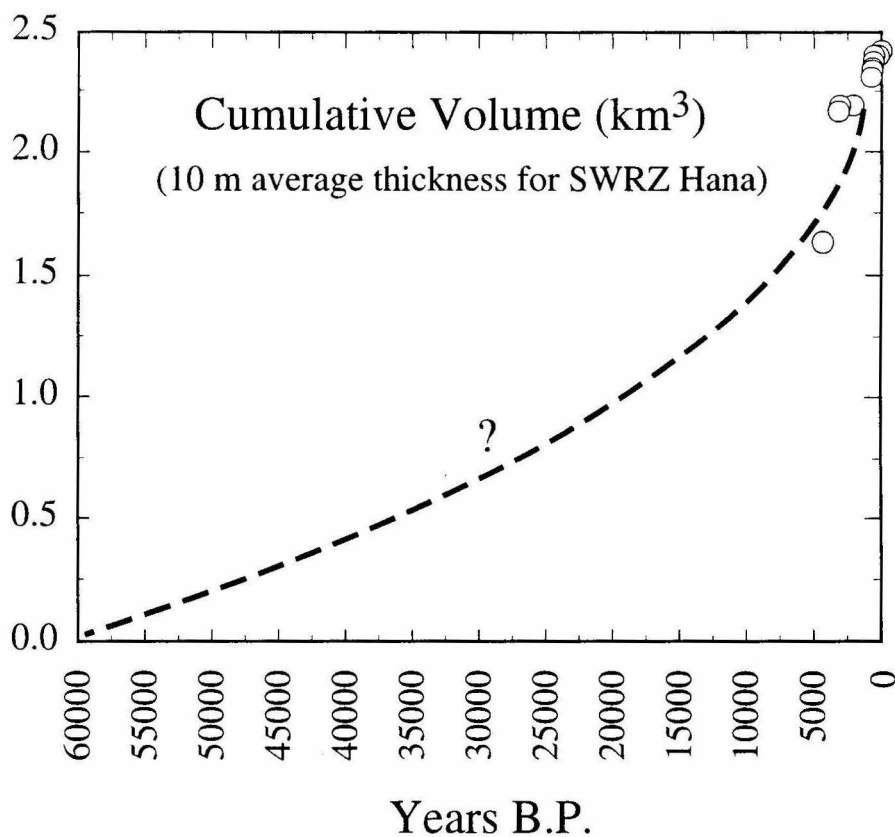
Figure 9.   Cumulative volume of southwest rift zone lavas versus time.
Total cumulative volume for southwest rift zone Hana calculated
from total outcrop area and an assumed average thickness of 10 m.

37

confined primarily to the central rift zone. Similar petrographically as well as chemically, these felsic lavas represent some of the largest volume events that have been documented on the southwest rift zone. The two eruptive events that took place on the upper rift zone during this time period, the older being an evolved lava, were much smaller volumetrically than those erupted from the central rift zone. The lava flow age map and compositional data also show that five eruptive events producing very phyric ankaramitic lavas took place on the upper southwest rift zone centered ~2,000 yrs. B.P., followed by a period of quiescence of ~1,000 yrs. Volcanic activity resumed again ~830 cal yrs B.P. and eight eruptions took place over a period of ~600 yrs with the most recent being the ca. 1790 A.D. eruptive event. This most recent set of eruptions were broadly distributed along the rift zone axis with one off-axis eruption, and the lavas erupted were primarily ankaramites and alkalic basalts. However, the most evolved Hana lava yet documented from the southwest rift zone (hkhh, ~600 cal yrs B.P.) was erupted during this period. The average time interval between eruptions during the most recent pulse of volcanic activity was only ~75 years. Thus, the eruptive activity on the southwest rift zone over the last 4,500 yrs occurred in four episodes, each lasting from ~200-700 yrs separated by quiescent periods ~500-1000 yrs long. The older three of these episodes were spatially restricted but activity of the most recent episode was distributed along nearly the entire length of the southwest rift zone.

Spatial variation in lava composition

The vent locations for Hana Volcanics eruptive events were recorded to see if there are systematic compositional variations in southwest rift zone lavas with respect to their areal distribution. Vent locations are estimated for those lavas whose vents have been obscured by the products of later eruptive events. When major and trace elements are plotted versus vent location as a function of distance from the summit of East Maui, the data shows a broad scatter (Figure 12). The composition of on-axis and off-axis groups
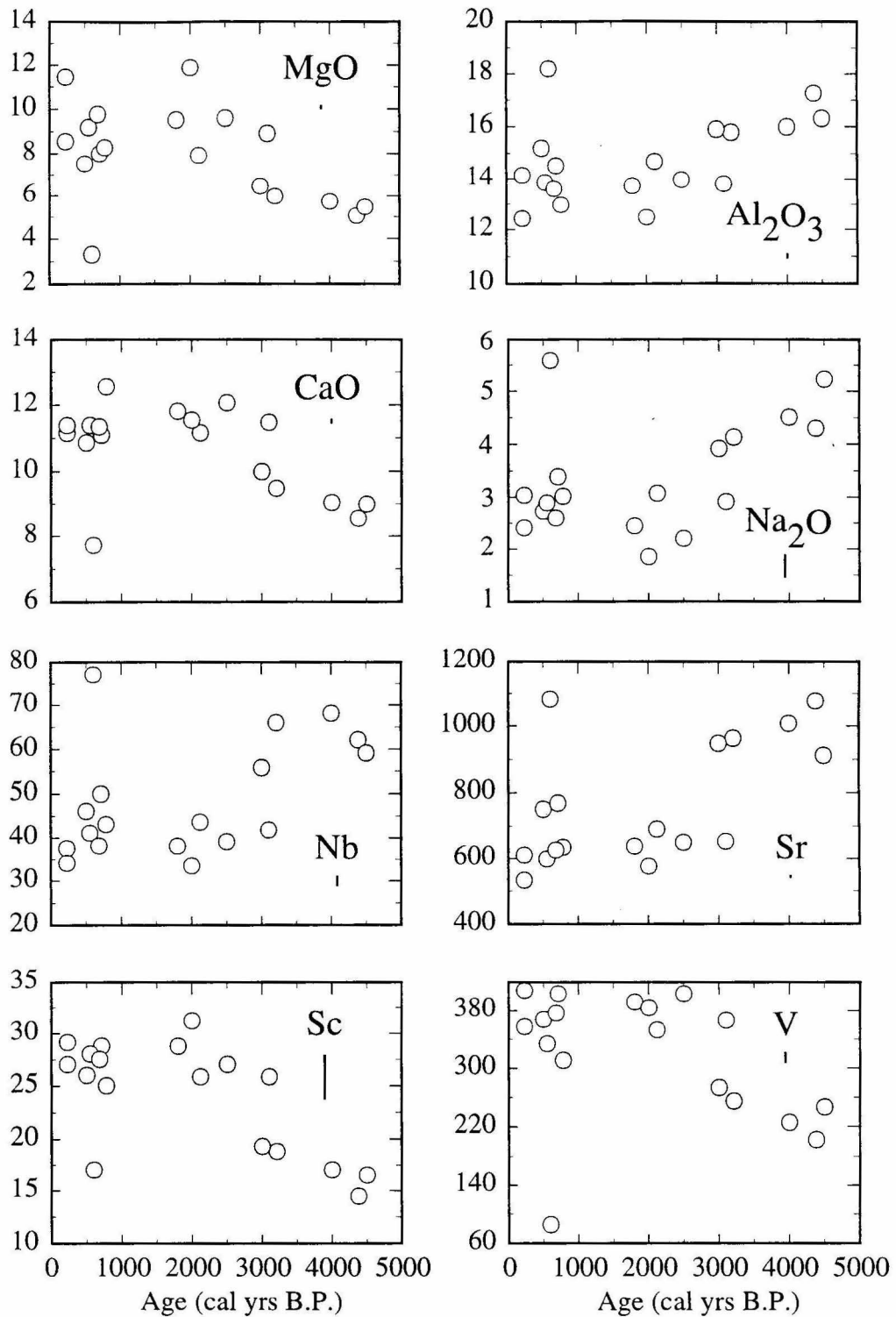
38

Figure 10. Selected major (wt.%) and trace element (ppm) abundances versus time for all southwest rift zone Hana lavas erupted within the last ~5000 yrs. Highly differentiated lavas were erupted ~3000-4500 yrs B.P.
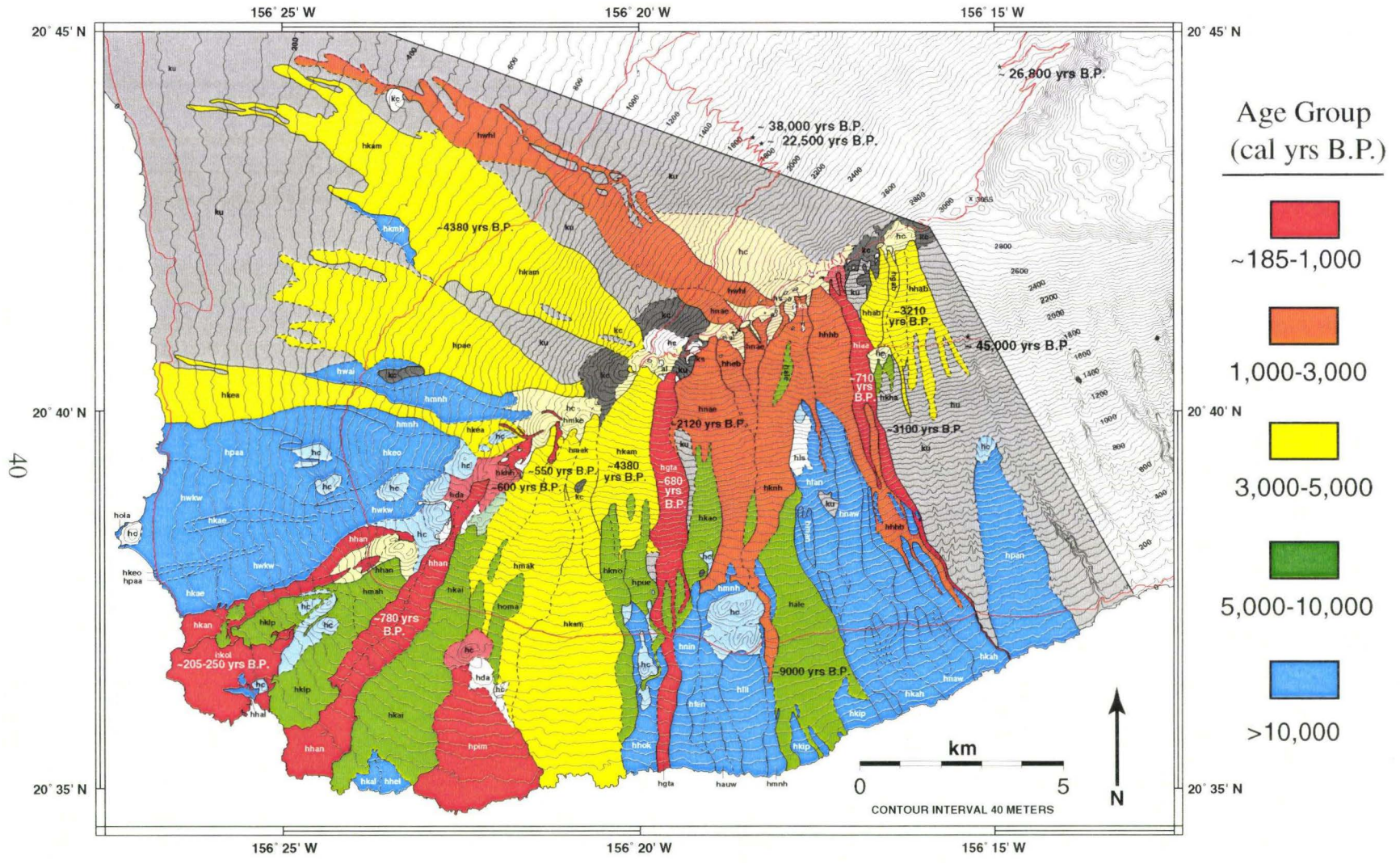
39

Figure 11. Lava flow age map for southwest rift zone Hana Volcanics. [14]C ages of lava flows and pyroclastics are posted where known. Post-shield Kula lavas and pyroclastics shown in gray.

overlap considerably, though none of the eight off-axis lavas are as evolved as the most evolved on-axis lavas. The plots also show that fairly unevolved lavas may erupt from any part of the rift zone, but the most evolved lavas have been erupted primarily from the central southwest rift zone. As discussed above, these evolved lavas were produced during large volume eruptions ~3000-4500 cal yrs B.P. Taken together, the data indicate little to no relationship between magma composition and eruption location on the axis and flanks of the southwest rift zone.

Volcanic hazards

Our improved understanding of the distribution and timing of Hana Volcanics eruptive events permits a new assessment of volcanic hazards along the southwest rift zone. Most Hawaiian volcanic eruptions produce lava flows that primarily endanger property; explosive eruptions that are more likely to threaten people are relatively rare. As land use on the flanks of the southwest rift zone becomes more intense through developments in agriculture, tourism, and residential areas, the threat to property and life will increase accordingly.

More than 90% of southwest rift zone lava flows can be characterized as a'a flows. Rough, rubbly surfaces and lava channels are ubiquitous features on most of the lava flows. Rowland and Walker (1990) concluded that high volumetric flow rate is an influential factor in the production of a'a flows by promoting efficient cooling and degassing, with corresponding increases in viscosity, in open lava channels and on the flow front itself. At high volumetric flow rates, lava continues to move quickly even after its viscosity and yield strength have increased significantly. Surface disruptions caused by shear forces on the lava within an open channel cannot be repaired by the high-viscosity lava beneath the surface, and a rubbly a'a flow results. They found that in Hawaiian lavas, when the volumetric flow rate was greater than ~5-10 m^3/sec, a'a lava formed; lower flow
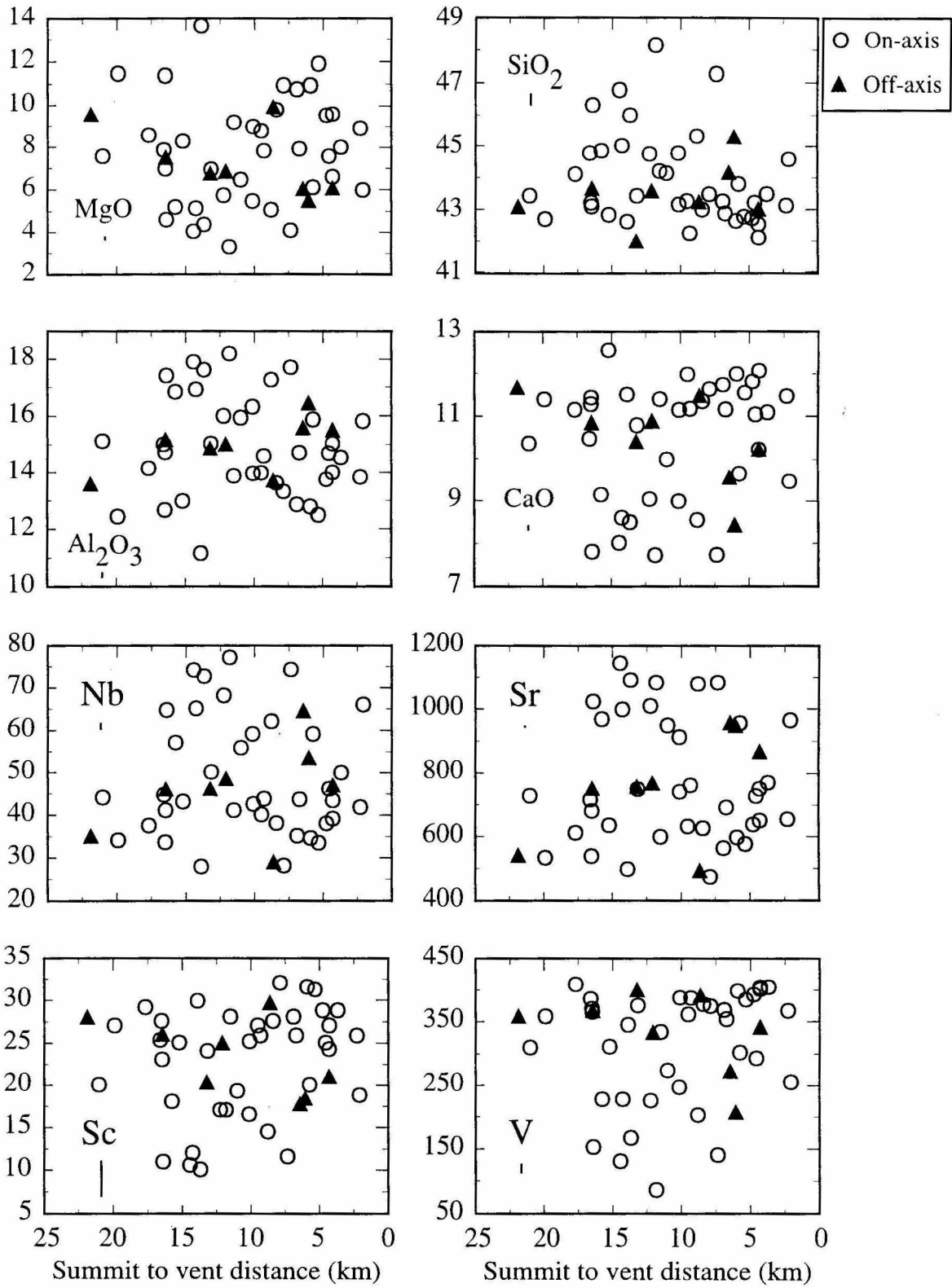
41

Figure 12.   Selected major (wt.%) and trace element (ppm) abundances versus vent
location as a function of distance from summit (km). There is no
systematic spatial variation in lava composition.

42

rates resulted in the formation of pahoehoe lava. Volumetric flow rate is generally controlled by effusion rate at the vent. Taken together, the prevalence of a'a flows and large cinder cones along the southwest rift zone suggests that the eruptions producing them were characterized by fire fountaining and effusion rates of greater than ~5-10 m^3/sec.

Slopes on the flanks of the southwest rift zone of East Maui are generally steeper than those of Mauna Loa and Kilauea on the Island of Hawaii (Mark and Moore, 1987). Although slopes vary considerably with location, much of the subaerial shields of Mauna Loa and Kilauea have average slopes of 3°-6°. Slopes on the south flank of the southwest rift zone of East Maui gradually decrease from a maximum of ~15° below the upper rift zone to ~10° for the slopes below the lower rift zone. On the north flank, slopes generally are not as great as those on the south flank, varying from ~10° below the upper southwest rift zone to ~8° for slopes below the lower rift zone, presumably due to northward moving lavas banking against the older West Maui volcano. Slopes generally are greater near the rift zone axis and decrease slightly with decreasing elevation; this feature is more pronounced on the north flank. Although slopes along the axis of the southwest rift zone vary with topographic features, the overall slope from summit to sea level is ~8°. Lava flows from the upper and central rift zone tend to travel downslope roughly perpendicular to the rift zone axis (Figure 1), reflecting the slope contrast between flanks and rift zone axis. On the lower rift zone, however, as flank slopes more closely approach the rift zone axis slope, lavas tend to travel downslope diagonally away from the vent or in some cases (hkol, hkan), almost along the rift zone axis.

Volumetric flow rate, flow front width, and slope all have an affect on flow front velocities in Hawaiian a'a flows. Flow front velocity observed in a'a flows varies from a few tens of meters per hour to almost 10,000 meters per hour (Macdonald and Finch, 1950; Lipman and Banks, 1987). Since most of the lava flows from the southwest rift zone are a'a, flow front velocities for these flows may be comparable to those observed on

43

Mauna Loa and Kilauea. Although the highest volumetric flow rates observed on Mauna Loa, producing some of the fastest moving flow fronts, are perhaps greater than those producing Hana a'a lavas, the steep flank slopes along the southwest rift zone may increase average flow front velocities. Distance from vent to coastline for eruptions from the southwest rift zone range from 0-20 km. Even when the highest flow front velocities are excluded, this suggests that travel time for a'a flows from the vent to the coast ranges from several hours to several days.

As discussed above, the chemical compositions of Hana lavas are consistent with them having undergone evolutionary processes at a depth of 10-11 km. If relatively small volumes of magma are ascending from this depth to the surface, there may be little precursory seismic activity prior to eruption (Moore et al., 1987). In addition, the East Maui Volcano is not monitored for seismic or deformation activity as intensely as its more active neighbors Kilauea and Mauna Loa. Taken together, this suggests that little warning will be available before eruptive activity on East Maui begins.

Although pyroclastic fall deposits in Hawaii, typically composed of cinder and ash, are not as destructive as lava flows, if accumulated in sufficient thickness they may temporarily render valuable land unusable and may bury or burn man-made structures. Pyroclastic fall deposits are typically thickest near the vent and thin rapidly with increasing distance. The hazard from pyroclastic material is greatest along the axis of the southwest rift zone where most eruptive vents are located and accumulations of bombs, cinder, and ash are likely to be the thickest (Moore et al., 1987). Because prevailing winds typically blow to the northwest across the rift zone axis, the pyroclastic fall hazard for the north flank of the southwest rift zone is much greater than the south flank. Fall deposits are pervasive on the north flank of the lower rift zone, fine cinder deposits as much as a meter thick have been found 3-4 km from the rift zone axis. Fall deposits on the south flank are limited primarily to areas immediately around and downwind of off-axis eruptive centers.

44

The three hazard zones shown on the lava flow hazards map for the southwest rift zone (Figure 13) do not differ significantly in size, areal extent, and ranking from those outlined by Crandell (1983) and Mullineaux et al. (1987). However, the descriptions of hazard zones in this study reflect an increased level of understanding of the timing of volcanic activity and areas covered by lava flows in this region. The hazard zone map distinguishes areas in which the general level of hazard is different from that of adjacent areas. However, the level of hazard may vary within a specific zone. Volcanic hazards generally decrease with increasing distance from an active vent, and local variations in topography may make one area more susceptible to flow coverage than another, even within the same zone. The change in degree of hazard between zones is generally gradual and may be apparent only over a few kilometers. Although hazard zones on the map are separated by relatively thin lines, changes in the degree of hazard between zones are gradual enough that they might be shown more appropriately by a continuous change in shading.

Hazard zone 1 includes an area in which there have been at least five eruptions within the last 1,000 years, and greater than 50% of the land surface has been covered by lava flows within the last 5,000 years. Hazard zone 1 covers the axis of the southwest rift zone and becomes larger at lower elevations reflecting the number of eruptions that have affected this area within the last ~1,000 years, and the less well-defined nature of vent distribution on the lower southwest rift zone.

Hazard zone 2 includes an area in which there has been at least one eruption within the last 1,000 years, and 30-50% of the land surface has been covered by lava flows within the last 5,000 years. Zone 2 covers the southern flank of the central and upper southwest rift zone and reflects the distribution of volcanic vents, and therefore lava flows, on the southern side of the topographic axis along the upper southwest rift zone.

Figure 13.   Southwest rift zone lava flow hazard zone map. See text for description of the numbered zones.

Hazard Zone 3 includes areas in which there has been no volcanic activity within the last 1,000 years, and less than 30% of the land surface has been covered by lava flows within the last 5,000 years. This zone covers the northern flank of the southwest rift zone and the area on the southern flank where the Lualailua Hills cinder cone complex forms a topographic barrier significantly decreasing the likelihood of future coverage by lava flows.

Lava flow hazard zones for the southwest rift zone of East Maui are compared with those defined by Mullineaux et al. (1987) on the Island of Hawaii in Table 6. Hazard zone rankings between the two areas do not correspond exactly because of the overall greater degree of hazard on the Island of Hawaii. Frequency of eruptions and percentage of lava flow cover within zones of similar hazard correspond only approximately with similar data on the other island. The hazard for Zone 1 on the axis of the southwest rift zone is roughly comparable to Zone 3 on the Island of Hawaii which includes the northwest and east flanks of Mauna Loa, and the north flank of Kilauea. Zone 3 on the southwest rift zone is roughly comparable to Zone 7 on Hawaii which includes the summit and upper flanks of Mauna Kea.

Table 6. Comparison of lava-flow hazard zones on the southwest rift zone of East Maui and the Island of Hawaii. (N.R., not represented)

Southwest Rift Zone	Island of Hawaii
N.R.	1
N.R.	2
1	3
2	4
N.R.	5
N.R.	6
3	7
N.R.	8
N.R.	9

Although the hazards posed by eruptions from the southwest rift zone vary with location, the risks for the entire area must be considered quite low and do not vary a great deal within the hazard map area because of differing extents of development and land use. The areas with the highest hazard rating, the rift zone axis and south flank, are nearly unpopulated and have been little developed. The combination of young, rough lava flow surfaces, an almost complete lack of arable land, and dry climate are likely to ensure that the rift zone axis and south flank are populated only by a few hardy homesteaders and used in a limited capacity as cattle grazing land in the foreseeable future. Although development and land use is greater on the north flank, especially the resort areas along the west coast between Makena and Kihei, the threat posed by volcanic hazards is generally lower than in hazard zones 1 and 2. Thus, the risk from volcanic hazards on the north flank of the southwest rift zone is similar to that of the axis and south flank.

CONCLUSIONS

Rejuvenated (Hana) volcanism along the southwest rift zone of East Maui began ~60,000 yrs B.P. ± 15,000 yrs. A ~50,000 minimum onset age implies that the period of quiescence between post-shield and rejuvenated stages on East Maui is no longer than 310,000 yrs, the shortest yet documented on any Hawaiian volcano.

Southwest rift zone Hana lavas are derived from similar parental magmas and related by varying degrees of fractional crystallization. Crystallization simulations suggest that evolutionary processes are occurring at a pressure of ~3 kbar, corresponding to a depth of ~10-11 km.

Overall eruption frequency and erupted volume of the Hana Volcanics along the southwest rift zone has increased through time, dramatically so in the last ~4400 yrs.

Volcanic activity on the southwest rift zone may occur in discrete episodes, with each episode lasting several hundred to about 1,500 years. Several eruptions occur relatively closely spaced in time producing lavas of similar composition, and volcanic events within these episodes may or may not be spatially restricted to a localized area on the rift zone.

The southwest rift zone poses a small but real volcanic hazard to those living and working on its flanks.

Appendix A. Sample locations of Southwest rift zone Hana Volcanics.

EMH-1   hhab, olivine phyric basanite. Center of lava flow, 2780 m elevation, 0.62 km
         S 11° W of radio tower at 2985 m. (USGS Lualailua Hills Quadrangle)

EMH-2   hhab, olivine phyric basanite. 100 m west of contact with newer member of
         hhab, 2735 m elevation, 0.93 km S 25° W of radio tower at 2985 m.

EMH-3   hgab, ankaramite basanite. Center of flow, 0.2 km S of vent, 2750 m
         elevation 1.1 km S 32° W of radio tower at 2985 m.

EMH-4   hknh, Kanahau ankaramite basanite. Eastern margin of flow, contact with hc,
         Hana cinder, 2530 m elevation, 0.29 km S 25° E from summit of Kanahau at
         2660 m.

EMH-6   hhhb, ankaramite picro-basalt. Eastern margin of flow, contact with hc, 2570
         m elevation, 0.53 km S 88° E from summit of Kanahau at 2660 m. ·

EMH-7   hlaa, Laau sparsely phyric ankaramite basanite. Near eastern margin of flow,
         0.30 km S 10° E of vent, 2155 m elevation, 0.75 km S 12° W from summit of
         Kalepeamoa.

EMH-8   hhan, Hanamanioa ankaramite basanite. Vesicular pahoehoe, 5 m elevation,
         0.16 km due E of Hanamanioa Light (USGS Makena Quadrangle).

EMH-9   hkai, Kaimaloo aphyric basanite. Sample taken near lower foot trail, 13 m
         elevation, 1.88 km N 86° E of Kamanamana Pt.

EMH-10   hhel, aphyric basanite, source unknown. Sample taken near lower foot trail,
         15 m elevation, 1.70 km N 82° E of Kamanamana Pt.

EMH-11   hkal, Kaloi olivine phyric basanite, source unknown. Sample taken near
         lower foot trail, 6 m elevation, 0.46 km N 57° E of Kamanamana Pt.

EMH-13   hhan, Hanamanioa ankaramite basanite. Center of flow several m makai of
         lower foot trail, 18 m elevation, 0.64 km N 20° E of Hanamanioa Light.

EMH-14   hhan, Hanamanioa ankaramite basanite. 100 m east of western flow margin
         on 4WD trail, 3 m elevation, 1.13 km N 5° W of Hanamanioa Light.

EMH-15   hklp, Kalualapa ankaramite picro-basalt, source unknown. Center of flow on
         4WD trail, 3 m elevation, 0.73 km S 26° E from summit of Puu o Kanaloa.

EMH-16   hknl, Puu O Kanaloa scoria, olivine phyric basanite. Sample taken from
         flank of cinder cone, 25 m elevation, 0.15 km S 45° W from summit of Puu o
         Kanaloa.

EMH-17   hhal, Halua olivine phyric basanite, source unknown. Sample taken in dry
         forested kipuka several m mauka of road, 18 m elevation, 0.34 km S 76° W
         from summit of Puu o Kanaloa.

EMH-18   hkol, Kalua o Lapa ankaramite basanite. Center of flow several m mauka of
         road, 23 m elevation, 1.23 km N 56° W from summit of Puu o Kanaloa.

Appendix A. (Continued) Sample locations of Southwest rift zone Hana Volcanics.

EMH-19 hkan, Kanahena ankaramite basanite. Center of flow, several m mauka of road, 13 m elevation, 0.35 km NW of BM 48 on road.

EMH-20 hlll, Lualailua olivine phyric basanite. Sample taken several m SE of collapsed lava pond (eastern gravel pit), several m mauka of Piilani Hwy., 475 m elevation (USGS Lualailua Hills Quadrangle).

EMH-21 hkao, Kao aphyric basanite. Lava block in Lualailua Cone, collected a few m mauka of Piilani Hwy, 465 m elevation, S 15° W of 600 m VABM on Lualailua Cone.

EMH-22 hlll, Lualailua olivine phyric basanite. Collected from edge of gravel pit a few m mauka of Piilani Hwy, 465 m elevation, S 53° W of 600 m VABM on Lualailua Cone.

EMH-23 hkam, Kamaole aphyric basanite. Eastern flow margin, junction of Piilani Hwy. and 4WD trail, mauka side at 501 m (1645 ft) elevation marker, 0.56 km W of eastern edge USGS Makena Quadrangle.

EMH-24 hkam, Kamaole aphyric basanite. Center of flow, several m mauka of Piilani Hwy., 550 m elevation, 1.33 km W of 501 m (1645 ft) elevation marker.

EMH-25 hmak, Makua olivine phyric basanite. Sample taken 130 m E of contact with unit homa, 40 m mauka of Piilani Hwy., 561 m elevation, 0.65 km E of junction Piilani Hwy. and Kanaio 4WD trail.

EMH-26 hhan, Hanamanioa ankaramite basanite. Center of flow, several m mauka of lower Puu Mahoe dirt road, 622 m elevation, 0.15 km SE of junction Piilani Hwy. and lower Puu Mahoe dirt road.

EMH-27 hhan, Hanamanioa ankaramite basanite. Sample collected several m W of cinder pit mauka of lower Puu Mahoe dirt road, 674 m elevation.

EMH-28 hmah, Mahoe ankaramite basanite. Sample taken from flow in Puu Mahoe cone, several m mauka of lower Puu Mahoe rd, 710 m elevation, 0.39 km S 16° W of radio facility at summit of Puu Mahoe.

EMH-29 hhan, Hanamanioa ankaramite basanite. Sample taken from roadcut 50 m E of Ulupalakua Ranch gate on Kanaio dirt road, 735 m elevation, 0.74 km S 75° E of Puu Mahoe radio facility.

EMH-30 hhan, Hanamanioa ankaramite basanite. Sample taken from mauka side of roadcut, Kanaio dirt road, 740 m elevation, 1.1 km S 72° E of Puu Mahoe radio facility.

EMH-31 hkai, Kaimaloo aphyric basanite. Sample collected from mauka side of roadcut, Kanaio dirt road, 720 m elevation, 0.7 km N 27° W of Kanaio Church.

EMH-33 hola, Olai ankaramite basanite. From flow unit exposed at base of Puu Olai cinder cone, 3 m elevation, 0.36 km N 32° W from summit of Puu Olai.

Appendix A. (Continued) Sample locations of Southwest rift zone Hana Volcanics.

EMH-34   hpaa, Papaanui aphyric basanite. Sample collected from coastal road at Paako, 3 m elevation, 1.33 km S 28° E from summit of Puu Olai.

EMH-35   hpaa, Papaanui aphyric basanite. Sample collected from lava exposed at coast near Nahuna, 2 m elevation, 0.27 km N 11° W of Makena BM.

EMH-36   hkea, Keauhou aphyric basanite. Sample collected from roadcut at center of flow near Halo, 11 m elevation, 1.51 km N of Makena BM.

EMH-37   hkha, Kahua olivine phyric basanite. Sample taken from lava flow just S of Kahua cone, 2055 m elevation, 0.33 km S 30° E from summit of Kahua cone (USGS Lualailua Hills Quadrangle).

EMH-38   hlaa, Laau sparsely phyric ankaramite basanite. Sample collected from western flow margin on Kahua 4WD trail, 2170 m elevation, 1.0 km N 83° W from summit of Kahua cone.

EMH-39   hhhb, ankaramite basanite. Center of flow on Kahua 4WD trail, 2180 m elevation, 1.51 km due E from summit of Kahua cone.

EMH-40   hknh, Kanahau ankaramite basanite. Near western flow margin on Kahua 4WD trail, 2220 m elevation, 1.38 km S 21° W from summit of Kanahau.

EMH-41   hnae, Naenae ankaramite basanite. Eastern flow margin on Kahua 4WD trail, 2195 m elevation, 1.55 km S 32° W from summit of Kanahau.

EMH-42   hheb, ankaramite basanite. Eastern flow margin 150 m makai of Kahua 4WD trail, 2180 m elevation, 1.23 km N 87° E from Ball Park Junction.

EMH-43   hnae, Naenae ankaramite basanite. 100 m from western flow margin on Kahua 4WD trail, 2190 m elevation, 0.49 km N 75° E from Ball Park Junction.

EMH-46   hnae, Naenae ankaramite basanite. 130 mauka of Skyline 4WD trail, 2355 m elevation, 1.43 km N 59° E from Ball Park Junction.

EMH-47   hwhl, Waiohuli ankaramite picro-basalt. Makai side of Skyline 4WD trail, 2450 m elevation, 0.80 km S 57° W from summit of Kanahau.

EMH-48   hwhl, Waiohuli ankaramite picro-basalt. 150 m S 43° E from junction Waiohuli Trail and Waipoli Rd., 2005 m elevation.

EMH-49   hklp, Kalualapa ankaramite basanite. Mauka side of 4WD trail, 240 m elevation, 0.87 km N 60°W from summit of Puu Naio. (USGS Makena Quadrangle)

EMH-50   hmke, Makuakeiki sparsely phyric ankaramite basanite. From distal end of flow, 1390 m elevation, 0.87 km S 9°E from summit of Puu Makua.

Appendix A. (Continued) Sample locations of Southwest rift zone Hana Volcanics.

EMH-51   hkam, Kamaole aphyric basanite. Center of flow, 1740 m elevation, 0.75 km
          S 29° E from summit of Polipoli cone.

EMH-52   hkam, Kamaole aphyric basanite. 100 m from western flow margin, 1715 m
          elevation, 0.67 km S 5° W from summit of Polipoli cone.

EMH-53   hmak, Makua sparsely olivine phyric basanite. Mauka side of 4WD trail,
          1600 m elevation, 1.17 km N 87° E from summit of Puu Makua.

EMH-54   hmak, Makua sparsely olivine phyric basanite. Near vent, 1525 m elevation,
          0.71 km S 74° E from summit of Puu Makua.

EMH-55   hmak, Makua sparsely olivine phyric basanite. Center of flow, 1400 m
          elevation, 0.77 km S 4° E from summit of Puu Makua.

EMH-56   hkhh, Keonehunehune aphyric basanite. From distal flow lobe, 1295 m
          elevation, 0.36 km E from water tank on Keonehunehune.

EMH-57   hhan, Hanamanioa ankaramite basanite. 50 m from western flow margin, 960
          m elevation, 0.71 km N 61° W from summit of Kaimaloo cone.

EMH-58   hwkw, Waiokawa aphyric basanite. From center of flow, 760 m elevation,
          1.0 km N 58° E from junction Piilani Hwy. and lower Puu Mahoe dirt road.

EMH-59   homa, Old Makua olivine phyric basanite. A few NE from junction Piilani
          Hwy. and Kanaio jeep trail, 545 m elevation, 0.44 km S 37° E from Kanaio
          Church.

EMH-62   hhab, sparsely olivine phyric basanite. From center of flow, 2785 m
          elevation, 1.2 km S 45° W of radio tower at 2985 m. (USGS Lualailua Hills
          Quadrangle)

EMH-63   hkno, Kanaio olivine phyric basanite.   A few m mauka of Piilani Hwy., 500
          m elevation, 0.31 km W from junction Makawao/ Hana District boundary and
          Piilani Hwy. (USGS Makena Quadrangle)

EMH-64   hkao, Kao aphyric basanite. A few m mauka of Piilani Hwy., 490 m
          elevation, 1.08 km N 37° E from summit of Hokukano cone. (USGS
          Lualailua Hills Quadrangle)

EMH-65   hnin, Ninialii ankaramite basanite. A few m mauka of Piilani Hwy., 485 m
          elevation, 1.22 km N 45° E from summit of Hokukano cone.

EMH-66   hmnh, Menehune ankaramite basanite. A few m mauka of Piilani Hwy., 460
          m elevation, 0.62 km W from 598 m VABM on Lualailua Hills.

EMH-67   hnae, Naenae ankaramite basanite. A few m mauka of Piilani Hwy., 460 m
          elevation, 0.84 km W from 598 m VABM on Lualailua Hills.

EMH-68   hale, Alena aphyric basanite. A few m mauka of Piilani Hwy., 460 m
          elevation, 1.66 km N 86° E from 598 m VABM on Lualailua Hills.

Appendix A. (Continued) Sample locations of Southwest rift zone Hana Volcanics.

EMH-69   hman, Manukani ankaramite basanite. A few m NE of junction Piilani Hwy. and 4WD trail, 420 m elevation, 1.61 km S 70° W from Kahikinui House.

EMH-70   hkah, Kahikinui sparsely olivine phyric basanite. A few m mauka of Piilani Hwy., 395 m elevation, 0.88 km S 51° W from Kahikinui House.

EMH-71   hnaw, Nawini ankaramite basanite. A few m mauka of Piilani Hwy., 350 m elevation, 0.42 km S 5° W from Kahikinui House.

EMH-72   hkah, Kahikinui sparsely olivine phyric basanite. A few m mauka of Piilani Hwy., 330 m elevation, 0.58 km S 33° E from Kahikinui House.

EMH-82   hkam, Kamaole aphyric basanite. A few m mauka of Piilani Hwy., 870 m elevation, 1.05 km S 45° W of Kula Hospital. (USGS Makena Quadrangle)

EMH-86   hnae, Naenae ankaramite basanite. From ponded lava in vent area, 2255 m elevation, 1.82 km S 55° W from 2638 m VABM on Kanahau cone. (USGS Lualailua Hills Quadrangle)

EMH-91   hgta, Giant tumulus ankaramite basanite. 70 m from western flow margin, 1965 m elevation, 0.62 km S 17° E from 2078 m summit of Kamaole cone.

BEM-5   hkip, Kipapa ankaramite basanite. A few m mauka of lower foot trail (King's Trail), 15 m elevation, 50 m N 71° W from junction rock wall and lower foot trail near Kipapa point.

BEM-7   hkah, Kahikinui sparsely olivine phyric basanite. From western flow margin, 60 m elevation, 1.36 km due S from Gaging Station in Kepuni Gulch just above Piilani Hwy.

BEM-8a   hlaa, Laau sparsely phyric ankaramite basanite. In Kepuni Gulch, 60 m elevation, 1.10 km S 35° E from Gaging Station in Kepuni Gulch just above Piilani Hwy.

BEM-14   hmnh, Menehune ankaramite basanite. 50 m from eastern flow margin, 140 m elevation, 1.38 km N 46° W from 8 m VABM at Kiakeana Pt.

BEM-32   hmnh, Menehune ankaramite basanite. Near eastern flow margin, 685 m elevation, 0.55 km N 45° E from 731 m summit of Lualailua Hills.

BEM-33   hmnh, Menehune ankaramite basanite. 620 m elevation, 0.39 km N 70° W from 731 m summit of Lualailua Hills.

BEM-34   hnae, Naenae ankaramite basanite. Center of flow, 690 m elevation, 0.83 km N 48° E from 731 m summit of Lualailua Hills.

BEM-37   hpan, Pane aphyric basanite. From western edge of Palaha Gulch, 160 m elevation, 0.35 km N 72° W from 96 m BM on Piilani Hwy.

Appendix A. (Continued) Sample locations of Southwest rift zone Hana Volcanics.

BEM-39   hhab, olivine phyric basanite. From kipuka on 4WD trail, 900 m elevation, 1.87 km S 87° E from 1100 m summit of Manukani.

BEM-40   hnaw, Nawini ankaramite basanite. From 4WD trail, 920 m elevation, 1.72 km due E from 1100 m summit of Manukani.

BEM-42   hnaw, Nawini ankaramite basanite. From 4WD trail, 990 m elevation, 1.49 km N 82° E from 1100 m summit of Manukani.

BEM-43   hkam, Kamaole aphyric basanite. From eastern flow margin on 4WD trail, 1225 m elevation, 3.15 km N 33° W from 731 m summit of Lualailua Hills.

BEM-44   hgta, Giant Tumulus ankaramite basanite. From western flow margin on 4WD trail, 1230 m elevation, 3.08 km N 32° W from 731 m summit of Lualailua Hills.

BEM-48   hlan, olivine phyric basanite. 1060 m elevation, 0.25 km N79° E from 1100 m summit of Manukani.

BEM-56   hkam, Kamaole aphyric basanite. From 4WD trail, 840 m elevation, 2.80 km N 75° E from Kanaio Church (USGS Makena Quadrangle)

BEM-58   hpue, Pueo ankaramite basanite. From 4WD trail, 840 m elevation, 2.37 km km N 60° W from 731 m summit of Lualailua Hills. (USGS Lualailua Hills Quadrangle)

BEM-63   hpim, Pimoe olivine phyric basanite. A few m makai of lower foot trail, 50 m elevation, 2.06 km S 21° E from 367 m summit of Pohakea cone. (USGS Makena Quadrangle)

BEM-66   hkam, Kamaole aphyric basanite. From lower foot trail, 30 m elevation, 3.34 km S 53° E from 367 m summit of Pohakea cone.

BEM-69.   hgta, Giant Tumulus ankaramite basanite. From lower foot trail, 25 m elevation, 2.37 km S 12° E from 446 m VABM on summit of Hokukano cone. (USGS Lualailua Hills Quadrangle)

BEM-70   hhok, Hokukano aphyric basanite. From 4WD trail, 90 m elevation, 3.40 km S 65° E from 367 m summit of Pohakea cone. (USGS Makena Quadrangle)

BEM-71   hkno, Kanaio olivine phyric basanite. From 4WD trail, 205 m elevation, 3.43 km S 80° E from 367 m summit of Pohakea cone.

BEM-80.   hman, Manukani ankaramite basanite. From eastern flow margin off 4WD trail, 865 m elevation, 0.68 km S 27° E from 1100 m summit of Manukani. (USGS Lualailua Hills Quadrangle)

BEM-88   hkao, Kao aphyric basanite. A few m mauka of Forest Reserve fenceline, 1540 m elevation, 2.57 km N 59° W from 1100 m summit of Manukani.

Appendix A. (Continued) Sample locations of Southwest rift zone Hana Volcanics.

BEM-153   hpae, Paeahu aphyric basanite. From 4WD trail, 878 m elevation, 1.57 km N 43° E from 866 m summit of Puu Io. (USGS Makena Quadrangle)

BEM-163   hkeo, Keauhou ankaramite picro-basalt. A few m mauka of dirt road, 230 m elevation, 2.56 km N 73° E from 15 m BM at Nahuna Pt.

BEM-166   hkae, Kaeo olivine phyric basanite. From cinder quarry access road, 120 m elevation, 2.14 km N 85° E from 110 m summit of Puu Olai.

BEM-203   hmnh, Menehune ankaramite basanite. From southern flow margin, 745 m elevation, 1.56 km S 22° W from 866 m summit of Puu Io.

Appendix B. XRF precision and accuracy.

	Single runs of standard BHVO-1													Average	Std. Dev.	Accepted	Error
SiO_2	49.46	49.32	49.28	49.59	49.55	49.58	49.74	49.75	49.49	49.67	49.72	49.72	49.69	49.58	0.16	49.59	0.01
TiO_2	2.63	2.67	2.72	2.69	2.67	2.68	2.65	2.76	2.74	2.73	2.73	2.72	2.75	2.70	0.04	2.69	0.01
Al_2O_3	13.67	13.69	13.54	13.70	13.72	13.72	13.75	13.73	13.62	13.73	13.71	13.75	13.75	13.70	0.06	13.70	0.00
Fe_2O_3	12.38	12.35	12.42	12.39	12.38	12.39	12.39	12.42	12.45	12.44	12.43	12.42	12.43	12.41	0.03	12.39	0.02
MnO	0.16	0.17	0.17	0.17	0.16	0.16	0.16	0.16	0.16	0.16	0.17	0.17	0.16	0.16	0.01	0.17	0.01
MgO	7.18	7.23	7.17	7.22	7.17	7.17	7.20	7.20	7.30	7.23	7.22	7.24	7.35	7.22	0.05	7.22	0.00
CaO	11.36	11.32	11.41	11.32	11.38	11.37	11.41	11.40	11.45	11.39	11.40	11.39	11.43	11.39	0.04	11.32	0.07
Na_2O	2.23	2.33	2.38	2.24	2.20	2.25	2.24	2.38	2.67	2.52	2.53	2.51	2.88	2.41	0.20	2.24	0.17
K_2O	0.52	0.52	0.52	0.52	0.52	0.52	0.51	0.51	0.54	0.53	0.53	0.52	0.51	0.52	0.01	0.52	0.00
P_2O_5	0.28	0.27	0.27	0.27	0.28	0.28	0.28	0.28	0.27	0.28	0.27	0.27	0.27	0.27	0.01	0.27	0.00
Total	99.87	99.87	99.87	99.87	100.03	100.12	100.33	100.59	100.69	100.70	100.71	100.72	101.22	100.35		100.11	
Sc			34				35				32			34	2	32	2
V			325				315				313			318	6	317	1
Cr			287				288				293			289	3	289	0
Ni			116				112				112			113	2	121	8
Cu			137				133				136			135	2	136	1
Zn			103				106				105			105	2	105	0
Rb			9				9				9			9	0	10	1
Sr			388				387				388			388	1	390	2
Y			27				27				27			27	0	28	1
Zr			177				177				177			177	1	179	2
Nb			19				18				18			18	0	19	1
Ba			143				143				122			136	12	139	3

Accepted values for standard BHVO-1 are those listed in Govindaraju (1989).

Errors are listed as the difference between the accepted value and the average of all the analyses.

Appendix C. XRF analyses of Hana Volcanics lavas.

	EMH-1	EMH-2	EMH-3	EMH-4	EMH-6	EMH-7	EMH-11	EMH-18	EMH-19	EMH-23	EMH-26	EMH-27	EMH-28
Unit	hhab	hhab	hgab	hknh	hhhb	hlaa	hkal	hkol	hkan	hkam	hhan	hhan	hmah
Rock Type	Ol	Ol	Ank	Ank	Ank	Ank	Ol	Ank	Ank	Aph	Ank	Ank	Ol
SiO_2	44.84	44.90	43.36	42.76	42.56	43.95	44.80	42.73	44.13	45.17	42.60	42.85	43.12
TiO_2	3.32	3.39	3.05	3.26	3.31	3.16	2.98	2.95	2.89	3.35	3.60	3.61	3.33
Al_2O_3	15.98	15.79	13.81	13.38	13.98	15.05	14.98	12.41	14.13	17.36	12.84	13.00	14.70
Fe_2O_3*	14.53	14.58	15.38	15.50	16.11	15.23	14.38	15.08	14.23	13.33	14.87	14.91	15.44
MnO	0.20	0.20	0.19	0.19	0.20	0.20	0.18	0.18	0.19	0.20	0.20	0.19	0.18
MgO	5.91	6.06	9.01	9.52	9.56	7.51	7.83	11.42	8.53	4.61	8.15	8.04	6.94
CaO	9.45	9.63	11.53	11.81	12.05	10.76	10.46	11.37	11.13	8.39	12.48	12.50	11.41
Na_2O	4.11	4.00	2.73	2.57	2.19	3.46	3.28	2.40	3.03	4.83	3.05	3.26	2.90
K_2O	1.68	1.61	0.97	0.90	0.67	1.22	1.05	0.87	1.11	1.78	1.25	1.28	1.05
P_2O_5	0.71	0.70	0.43	0.41	0.43	0.51	0.50	0.34	0.44	0.71	0.51	0.53	0.43
Total	100.74	100.86	100.47	100.30	101.06	101.06	100.45	99.76	99.79	99.73	99.56	100.17	99.50
H_2O	0.24	0.28	0.29	0.19	1.07	0.08	0.90	0.07	0.16	0.11	0.20	0.11	0.13
CO_2	0.04	0.01	0.06	0.06	0.09	0.04	0.06	0.09	0.02	0.07	0.16	0.12	0.07
Sc	19	21	28	28	27	25	25	27	25	14	31	31	23
V	251	258	345	386	403	324	292	357	310	180	406	406	364
Cr	55	60	340	395	311	169	274	549	389	5	305	283	138
Ni	43	46	118	160	134	81	105	277	152	5	135	129	84
Cu	94	74	89	75	61	71	77	112	117	25	166	173	77
Zn	119	119	108	104	113	117	103	103	106	114	111	110	108
Rb	42	41	24	22	16	29	22	22	28	40	29	29	27
Sr	962	954	623	625	649	738	726	532	633	1172	762	770	678
Y	32	32	27	26	27	29	28	25	27	33	26	27	28
Zr	291	286	194	184	192	227	207	165	199	269	232	234	196
Nb	66	65	40	37	39	47	46	34	43	69	49	50	41
Ba	746	738	447	435	474	566	560	417	485	835	528	519	491

*Total iron is listed as Fe_2O_3

Appendix C. (Continued) XRF analyses of Hana Volcanics lavas.

	EMH-29	EMH-30	EMH-31	EMH-41	EMH-42	EMH-43	EMH-45	EMH-46	EMH-48	EMH-49	EMH-50	EMH-51	EMH-52
Unit	hhan	hhan	hkai	hnae	hheb	hnae	hgta	hnae	hwhl	hklp	hmke	hkam	hkam
Rock Type	Ank	Ank	Aph	Ank	Ank	Ank	Ank	Ank	Ank	Ank	Ank	Aph	Aph
SiO_2	43.06	42.93	46.49	42.91	43.28	42.74	42.78	42.90	43.06	43.15	44.23	45.38	45.40
TiO_2	3.67	3.65	3.06	3.52	2.86	3.45	3.10	3.49	2.75	2.78	2.92	3.37	3.38
Al_2O_3	13.08	13.03	17.69	14.71	12.84	14.64	13.34	14.68	12.31	12.25	13.85	17.06	17.22
Fe_2O_3*	15.06	14.93	12.79	15.76	15.25	15.71	15.74	15.71	15.01	14.95	14.52	13.99	13.98
MnO	0.19	0.19	0.20	0.19	0.19	0.19	0.19	0.19	0.18	0.19	0.19	0.19	0.19
MgO	8.34	8.28	4.25	7.98	10.71	8.08	10.12	8.03	11.92	11.94	9.16	5.26	5.15
CaO	12.41	12.59	8.01	11.26	11.71	11.22	11.42	11.24	10.99	10.97	11.37	8.66	8.49
Na_2O	3.06	3.31	5.15	3.07	2.64	2.99	2.56	2.98	2.37	2.39	2.88	4.18	4.29
K_2O	1.28	1.30	1.90	1.04	0.90	1.04	0.85	1.06	0.88	0.85	1.05	1.65	1.62
P_2O_5	0.52	0.52	0.81	0.48	0.38	0.47	0.40	0.48	0.35	0.35	0.41	0.60	0.61
Total	100.68	100.73	100.36	100.93	100.76	100.53	100.51	100.77	99.83	99.82	100.59	100.34	100.34
H_2O	0.19	0.14	0.15	0.20	0.27	0.22	0.31	0.22	0.07	0.10	0.08	0.60	0.28
CO_2	0.14	0.03	0.03	0.09	0.03	0.03	0.08	0.06	0.03	0.08	0.01	0.02	0.04
Sc	27	28	12	26	28	25	27	25	29	27	28	15	15
V	380	389	139	378	367	372	343	376	363	335	333	195	197
Cr	196	277	<3	211	477	212	346	211	551	672	434	6	5
Ni	119	133	6	80	202	86	123	83	210	333	175	9	6
Cu	129	122	25	47	65	43	50	45	61	113	99	32	29
Zn	109	110	118	110	105	110	106	114	101	105	109	103	102
Rb	30	29	46	25	22	26	20	25	19	22	26	37	38
Sr	758	761	1107	750	562	739	636	742	574	525	597	1019	1035
Y	27	26	34	29	25	29	26	29	25	24	27	32	33
Zr	237	233	302	202	168	200	188	203	169	164	190	249	251
Nb	50	50	73	42	35	42	38	43	33	34	41	58	59
Ba	521	505	824	504	380	513	501	510	400	403	445	731	760

59

*Total iron is listed as Fe_2O_3

Appendix C. (Continued) XRF analyses of Hana Volcanics lavas.

	EMH-53	EMH-54	EMH-55	EMH-56	EMH-57	EMH-59		BEM-5	BEM-7	BEM-8A	BEM-14	BEM-30
Unit	hmak	hmak	hmak	hkhh	hhan	homa		hkip	hkah	hlaa	hmnh	hu
Rock Type	Ol	Ol	Ol	Aph	Ank	Ol		Ank	Ol	Ank	Ank	Aph
SiO_2	44.11	44.08	44.24	48.16	42.94	43.45		43.50	42.41	43.56	43.67	44.05
TiO_2	3.25	3.26	3.18	2.52	3.58	3.39		2.95	4.13	3.07	3.10	3.47
Al_2O_3	15.87	15.84	15.91	18.17	13.01	15.01		13.30	15.01	14.43	14.01	15.23
Fe_2O_3*	14.46	14.44	14.40	11.91	14.97	15.63		15.21	17.23	15.26	15.45	15.26
MnO	0.19	0.19	0.20	0.21	0.20	0.19		0.18	0.21	0.20	0.19	0.19
MgO	6.39	6.45	6.39	3.28	8.20	6.91		10.90	6.61	8.09	9.33	6.82
CaO	10.17	10.14	9.75	7.71	12.55	10.77		11.61	10.16	11.08	11.84	10.91
Na_2O	3.99	4.03	4.20	5.58	3.18	3.36		1.90	2.64	2.75	2.07	2.79
K_2O	1.43	1.44	1.49	0.20	1.28	1.24		0.61	1.14	1.10	0.94	1.34
P_2O_5	0.57	0.58	0.60	0.87	0.53	0.53		0.31	0.47	0.48	0.39	0.53
Total	100.44	100.45	100.37	98.61	100.45	100.49		100.46	100.01	100.01	100.97	100.61
H_2O	0.17	0.13	0.15	0.21	0.25	0.27	LOI[a]	0.18	-0.26	-0.45	-0.40	-0.46
CO_2	0.04	0.02	0.06	0.06	0.10	0.07						
Sc	19	19	19	17	29	24		32	26	26	31	25
V	277	268	267	85	404	374		373	377	364	409	369
Cr	116	118	111	5	249	107		490	5	211	341	53
Ni	49	54	56	<3	123	67		188	41	98	142	67
Cu	45	50	45	36	133	67		69	48	75	77	62
Zn	106	112	115	124	113	116		109	119	114	107	114
Rb	34	34	34	53	30	30		14	26	26	23	32
Sr	927	927	938	1081	773	747		472	740	686	566	738
Y	31	31	32	36	26	30		23	31	27	24	28
Zr	227	227	234	340	235	224		140	202	210	164	220
Nb	55	55	57	77	51	50		28	43	43	36	48
Ba	706	706	665	845	579	576		-	-	-	-	-

60

*Total iron is listed as Fe_2O_3
[a]LOI listed as total loss on ignition. Condition for ignition was 900°C for eight hours.

Appendix C. (Continued) XRF analyses of Hana Volcanics lavas.

	BEM-32	BEM-33	BEM-34	BEM-37	BEM-39	BEM-40	BEM-42	BEM-43	BEM-44	BEM-48	BEM-56	BEM-58	BEM-63
Unit	hmnh	hmnh	hnae	hpan	hhab	hnaw	hnaw	hkam	hgta	hlan	hkam	hpue	hpim
Rock Type	Ank	Ank	Ank	Aph	Ol	Ank	Ank	Aph	Ank	Ol	Aph	Ank	Ol
SiO_2	43.55	43.54	43.42	45.34	44.75	43.28	43.43	45.65	43.37	44.20	45.64	42.27	43.70
TiO_2	3.05	3.22	3.41	3.44	3.29	3.58	3.43	3.44	3.17	3.25	3.35	3.34	3.36
Al_2O_3	13.80	14.60	14.89	16.44	15.83	14.81	14.95	17.27	13.63	15.58	17.50	14.57	15.17
Fe_2O_3*	15.46	15.41	15.55	13.98	14.41	15.81	15.93	14.23	15.83	14.50	13.49	15.58	15.31
MnO	0.19	0.20	0.19	0.20	0.20	0.20	0.20	0.20	0.20	0.21	0.21	0.19	0.19
MgO	9.23	7.90	7.62	5.49	5.93	7.40	7.35	5.24	9.92	6.03	4.81	7.78	7.50
CaO	11.92	11.85	11.01	8.42	9.37	10.52	10.56	8.49	11.38	9.55	8.45	11.14	10.84
Na_2O	2.09	2.11	2.58	4.93	3.70	2.99	2.80	3.56	2.20	4.79	4.37	3.78	2.72
K_2O	0.95	0.96	1.19	1.54	1.67	1.23	1.23	1.61	1.00	1.64	1.78	1.12	1.19
P_2O_5	0.42	0.47	0.54	0.60	0.74	0.55	0.55	0.62	0.43	0.70	0.72	0.49	0.49
Total	100.65	100.26	100.40	100.35	99.88	100.37	100.42	100.28	101.11	100.43	100.33	100.25	100.47
LOI[a]	-0.26	0.42	-0.57	-0.60	-0.39	-0.64	-0.48	-0.03	-0.53	-0.41	-0.42	-0.64	-0.50
Sc	30	29	27	18	18	25	23	16	28	18	13	25	26
V	422	394	388	207	247	359	366	225	383	272	185	386	367
Cr	324	227	159	11	41	145	148	0	379	56	<2	204	187
Ni	141	101	82	21	45	93	91	9	128	45	11	76	83
Cu	67	65	67	28	55	87	79	29	46	52	21	39	58
Zn	120	114	123	105	119	124	119	109	117	120	116	120	113
Rb	23	23	30	35	42	30	30	37	24	42	41	27	29
Sr	597	651	776	948	973	771	741	990	617	956	1185	738	750
Y	26	28	29	33	32	29	28	32	25	31	33	28	29
Zr	178	195	219	241	290	229	221	245	187	286	261	204	196
Nb	38	40	46	53	67	48	46	58	38	64	68	42	42
Ba	-	-	-	-	-	-	-	-	-	-	-	-	-

61

*Total iron is listed as Fe_2O_3
[a]LOI listed as total loss on ignition. Condition for ignition was 900°C for eight hours.

Appendix C. (Continued) XRF analyses of Hana Volcanics lavas.

	BEM-66	BEM-69	BEM-70	BEM-71	BEM-80	BEM-88	BEM-153	BEM-163	BEM-166	BEM-203	EMH-8	EMH-9
Unit	hkam	hgta	hhok	hkno	hman	hkao	hpae	hkeo	hkae	hmnh	hhan	hkai
Rock Type	Aph	Ank	Aph	Ol	Ank	Aph	Aph	Ank	Ol	Ank	Ank	Aph
SiO_2	45.29	42.84	42.03	43.03	43.21	47.54	44.80	42.64	44.87	43.10	42.55	47.13
TiO_2	3.39	3.15	3.51	2.93	2.66	2.64	3.26	2.53	3.14	3.14	3.59	2.74
Al_2O_3	17.36	12.83	14.85	13.89	13.87	17.65	16.29	11.13	16.81	13.86	12.83	18.05
Fe_2O_3*	13.35	15.50	16.30	14.67	15.33	12.38	14.28	14.53	13.60	15.28	14.85	12.41
MnO	0.20	0.19	0.21	0.19	0.18	0.21	0.20	0.18	0.21	0.19	0.20	0.21
MgO	4.74	11.10	6.75	8.91	9.66	3.95	5.44	13.61	5.17	8.71	8.15	3.82
CaO	8.36	11.92	10.40	11.06	11.40	7.71	8.97	11.48	9.13	12.05	12.46	7.99
Na_2O	4.47	1.77	4.33	3.84	3.31	5.76	5.22	3.08	4.32	2.36	3.10	5.34
K_2O	1.80	0.80	1.24	1.12	0.78	1.88	1.56	0.72	1.74	0.97	1.27	1.92
P_2O_5	0.73	0.39	0.50	0.44	0.33	0.81	0.65	0.31	0.70	0.36	0.51	0.80
Total	99.69	100.47	100.10	100.07	100.72	100.52	100.65	100.21	99.67	99.99	99.51	100.41
LOI[a]	-0.38	-0.31	-0.79	-0.27	-0.14	-0.65	-0.60	-0.33	0.47	-0.01	-0.65	-0.41
Sc	13	32	20	24	29	9	16	30	12	28	27	9
V	190	403	399	362	389	124	246	344	227	408	395	120
Cr	<2	559	19	387	379	<2	24	758	39	352	247	6
Ni	10	196	55	154	152	4	30	312	28	121	128	4
Cu	21	56	55	68	61	16	42	69	30	89	119	18
Zn	115	115	123	111	111	123	117	101	121	105	112	118
Rb	41	20	29	28	19	52	39	17	44	27	29	47
Sr	1179	596	756	649	500	1082	910	496	996	608	762	1179
Y	33	24	28	27	25	35	33	21	33	25	26	35
Zr	264	174	208	189	148	322	275	139	273	175	234	294
Nb	69	35	46	41	29	72	59	28	65	37	50	75
Ba	-	-	-	-	-	-	-	-	789	425	532	874

62

*Total iron is listed as Fe_2O_3
[a]LOI listed as total loss on ignition. Condition for ignition was 900°C for eight hours.

Appendix C. (Continued) XRF analyses of Hana Volcanics lavas.

	EMH-10	EMH-13	EMH-14	EMH-15	EMH-16	EMH-17	EMH-20	EMH-21	EMH-22	EMH-24	EMH-25	EMH-33
Unit	hhel	hhan	hhan	hklp	hklp	hhal	hlll	hkao	hlll	hkam	hmak	hola
Rock Type	Aph	Ank	Ank	Ank	Ank	Ol	Ol	Aph	Ol	Aph	Ol	Ank
SiO_2	46.35	42.89	43.09	43.33	43.45	45.32	43.82	47.12	43.41	45.37	44.19	43.12
TiO_2	2.91	3.66	3.66	2.99	3.49	3.10	3.40	2.86	3.50	3.52	3.41	3.01
Al_2O_3	17.38	12.91	12.98	13.03	15.10	16.16	14.74	17.48	15.25	17.24	16.00	13.58
Fe_2O_3*	13.25	14.97	14.98	15.51	15.58	13.85	14.76	12.89	15.12	13.88	14.46	15.38
MnO	0.20	0.19	0.19	0.19	0.20	0.19	0.18	0.20	0.19	0.19	0.20	0.18
MgO	4.58	8.37	8.47	10.73	7.53	6.11	7.22	4.22	6.43	5.14	6.50	9.55
CaO	7.80	12.66	12.64	11.55	10.35	9.44	11.14	7.74	10.59	8.86	9.83	11.66
Na_2O	5.39	2.64	2.50	1.78	3.20	4.25	3.01	4.70	3.40	3.37	3.41	2.76
K_2O	1.80	1.28	1.31	0.83	1.15	1.54	1.20	1.92	1.30	1.54	1.50	0.94
P_2O_5	0.73	0.53	0.53	0.36	0.47	0.63	0.51	0.82	0.52	0.59	0.61	0.40
Total	100.37	100.11	100.33	100.32	100.52	100.59	99.98	99.95	99.71	99.72	100.09	100.58
LOI[a]	-0.38	-0.53	-0.61	-0.42	-0.55	-0.70	0.01	-0.02	-0.54	-0.35	-0.68	0.55
Sc	11	28	29	28	20	19	26	14	24	17	20	28
V	152	423	422	403	309	216	314	149	352	233	279	358
Cr	<2	223	231	457	167	117	179	7	42	8	117	281
Ni	7	122	121	189	73	57	87	11	59	12	58	138
Cu	26	120	123	62	30	50	82	35	61	27	45	63
Zn	110	116	122	120	107	113	100	116	110	116	116	101
Rb	44	30	31	21	26	39	30	49	31	35	35	21
Sr	1021	776	781	548	726	899	771	1048	764	1024	995	541
Y	32	26	26	24	29	32	29	34	30	31	31	25
Zr	278	235	236	164	197	268	222	320	228	241	230	170
Nb	65	49	50	33	44	59	47	76	50	58	56	35
Ba	-	-	-	-	480	689	565	820	556	-	-	394

*Total iron is listed as Fe_2O_3
[a]LOI listed as total loss on ignition. Condition for ignition was 900°C for eight hours.

63

Appendix C. (Continued) XRF analyses of Hana Volcanics lavas.

	EMH-34	EMH-35	EMH-36	EMH-37	EMH-38	EMH-40	EMH-47	EMH-58	EMH-62	EMH-63	EMH-64	EMH-65
Unit	hpaa	hpaa	hkea	hkha	hlaa	hknh	hwhl	hwkw	hhab	hkno	hkao	hnin
Rock Type	Aph	Aph	Aph	Ol	Ank	Ank	Ank	Aph	Ol	Ol	Aph	Ank
SiO_2	46.19	45.87	44.77	43.06	43.02	42.75	42.53	45.04	43.95	43.33	47.21	42.50
TiO_2	3.05	3.19	3.34	4.02	3.00	3.17	2.96	3.63	3.22	3.02	2.71	3.00
Al_2O_3	17.83	17.35	15.98	15.50	14.05	14.07	12.63	16.90	15.56	13.98	17.91	12.68
Fe_2O_3*	12.49	13.28	14.40	16.24	15.18	15.63	15.52	14.27	14.41	14.68	12.23	15.25
MnO	0.19	0.21	0.19	0.20	0.20	0.19	0.19	0.20	0.20	0.18	0.20	0.18
MgO	4.00	4.68	5.70	6.06	8.28	9.48	11.81	5.10	5.93	8.99	4.01	10.71
CaO	8.33	8.62	9.02	10.23	11.39	11.78	12.05	8.58	9.40	11.19	7.72	12.03
Na_2O	5.19	4.73	4.50	3.37	3.93	2.29	1.30	4.18	4.66	3.07	5.25	2.55
K_2O	1.89	1.85	1.73	1.14	1.09	0.89	0.57	1.54	1.63	1.08	1.91	0.83
P_2O_5	0.83	0.77	0.74	0.50	0.46	0.44	0.37	0.63	0.71	0.44	0.84	0.38
Total	99.99	100.56	100.37	100.32	100.58	100.68	99.94	100.07	99.68	99.96	99.99	100.11
LOI[a]	0.61	0.71	-0.65	0.05	-0.82	-0.59	0.55	0.11	-0.20	-0.25	-0.19	-0.47
Sc	9	11	17	21	26	29	33	18	17	28	12	31
V	141	191	225	341	369	397	404	227	261	369	145	391
Cr	4	22	49	19	271	344	598	<2	49	425	<2	529
Ni	<3	16	37	33	99	141	211	7	39	169	6	183
Cu	12	19	51	46	73	62	52	22	54	78	17	53
Zn	116	119	115	110	117	115	112	120	123	123	119	108
Rb	45	46	44	28	25	21	15	36	41	27	50	21
Sr	1155	1023	1007	867	644	648	576	966	962	656	1112	595
Y	35	34	33	32	27	26	24	33	31	26	33	24
Zr	312	292	301	221	202	189	168	247	288	192	320	176
Nb	75	70	68	47	41	39	34	57	65	42	74	34
Ba	814	796	789	577	-	-	-	-	-	-	-	-

*Total iron is listed as Fe_2O_3
[a]LOI listed as total loss on ignition. Condition for ignition was 900°C for eight hours.

64

Appendix C. (Continued) XRF analyses of Hana Volcanics lavas.

	EMH-66	EMH-67	EMH-68	EMH-69	EMH-70	EMH-71	EMH-72	EMH-82	EMH-86	EMH-91	EMH-101
Unit	hmnh	hnae	hale	hman	hkah	hnaw	hkah	hkam	hnae	hgta	hu
Rock Type	Ank	Ank	Ol	Ank	Ol	Ank	Ol	Aph	Ank	Ank	Ank
SiO_2	43.14	42.77	43.82	43.35	41.62	43.03	42.37	44.88	42.64	42.67	42.67
TiO_2	3.10	3.48	3.51	2.60	4.25	3.36	4.21	3.33	3.49	3.10	2.75
Al_2O_3	13.86	14.70	15.85	13.54	15.13	14.25	14.90	16.92	14.50	13.57	11.83
Fe_2O_3*	15.05	15.41	14.90	15.20	17.49	15.20	16.95	14.05	15.52	15.65	15.63
MnO	0.19	0.19	0.20	0.18	0.21	0.19	0.20	0.20	0.20	0.19	0.19
MgO	8.66	7.58	6.07	10.15	6.66	7.88	6.42	5.30	8.00	9.59	12.77
CaO	11.85	10.94	9.63	11.52	10.20	11.99	10.28	8.55	11.11	11.25	11.32
Na_2O	2.93	3.43	4.02	2.50	2.79	3.18	3.46	5.29	3.29	2.98	2.19
K_2O	0.98	1.17	1.50	0.71	0.98	1.05	1.17	1.64	1.02	0.98	0.76
P_2O_5	0.42	0.52	0.66	0.32	0.48	0.43	0.45	0.60	0.49	0.42	0.36
Total	100.18	100.19	100.16	100.07	99.81	100.56	100.41	100.73	100.26	100.40	100.47
LOI[a]	-0.32	-0.53	-0.48	-0.41	0.21	-0.56	-0.30	-0.08	-0.46	-0.62	0.19
Sc	31	25	20	30	22	28	25	13	27	27	31
V	404	389	301	392	404	428	420	210	411	369	384
Cr	299	154	31	454	12	218	10	<2	199	352	566
Ni	125	82	37	168	44	103	43	7	80	123	289
Cu	64	68	48	68	46	65	49	27	45	48	49
Zn	110	121	124	112	129	115	120	109	115	110	107
Rb	24	29	37	18	22	25	27	37	27	24	18
Sr	630	791	954	485	771	627	736	1007	755	632	529
Y	27	29	32	24	31	27	31	31	28	26	23
Zr	188	226	270	146	211	187	208	244	206	191	159
Nb	38	47	59	29	44	40	43	57	42	38	31
Ba	-	-	-	-	-	-	-	790	-	-	-

*Total iron is listed as Fe_2O_3

[a]LOI listed as total loss on ignition. Condition for ignition was 900°C for eight hours.

65

Appendix C. (Continued) XRF analyses of Hana Volcanics lavas.

	EMH-101	EMH-102	EMH-103
Unit	hu	hu	hu
Rock Type	Ank	Aph	Ank
SiO_2	42.67	44.44	42.94
TiO_2	2.75	3.94	3.07
Al_2O_3	11.83	16.55	13.81
Fe_2O_3*	15.63	14.15	15.33
MnO	0.19	0.19	0.20
MgO	12.77	5.58	8.75
CaO	11.32	9.23	11.36
Na_2O	2.19	4.16	3.08
K_2O	0.76	1.47	1.04
P_2O_5	0.36	0.61	0.45
Total	100.47	100.32	100.03
LOI[a]	0.19	0.04	-0.56
Sc	31	19	26
V	384	257	375
Cr	566	17	328
Ni	289	27	111
Cu	49	40	62
Zn	107	107	120
Rb	18	6	25
Sr	529	1045	636
Y	23	31	26
Zr	159	247	201
Nb	31	52	40
Ba	-	-	-

99

*Total iron is listed as Fe_2O_3
[a]LOI listed as total loss on ignition. Condition for ignition was 900°C for eight hours.

REFERENCES

Bard E., Arnold M., Fairbanks R.G, and Hamelin B. (1993) ^{230}Th-^{234}U and ^{14}C ages obtained by mass spectrometry on corals. Radiocarbon 35:191-199

Bender J.F., Hodges F.N., and Bence A.E. (1978) Petrogenesis of basalts from the project FAMOUS area: Experimental study from 0 to 15 kbars. Earth Planet Sci Lett 41: 277-302

Brill R.C. (1975) The geology of the lower southwest rift of Haleakala, Maui [Unpubl. M.S. thesis]: Honolulu, HI, University of Hawaii at Manoa, 65 p

Chappell B.W. (1991) Trace element analysis of rocks by x-ray spectrometry. Advances in X-ray analysis 34:263-276

Chen C.Y., Frey F.A. (1985) Trace element and isotopic geochemistry of lavas from Haleakala Volcano, East Maui, Hawaii: Implications for the origin of Hawaiian basalts. J Geophys Res 90:8743-8768

Chen C.Y., Frey F.A., Garcia M.O. (1990) Evolution of alkalic lavas at Haleakala Volcano, east Maui, Hawaii. Cont Min Petr 105:197-218

Chen C.Y., Frey F.A., Garcia M.O., Dalrymple G.B., and Hart S.R. (1991) The tholeiite to alkalic basalt transition at Haleakala Volcano, Maui, Hawaii. Cont Min and Petr 106: 183-200

Clague D.A. (1987) Hawaiian xenolith populations, magma supply rates, and development of magma chambers. Bull Volcanol 49:577-587

Clague D.A., Dalrymple G.B. (1987) The Hawaiian-Emperor Volcanic Chain. Part 1. Geologic evolution. US Geol Surv Prof Pap 1350:1-54

Clague D.A., Dalrymple G.B. (1988) Age and petrology of alkalic postshield and rejuvenated-stage lava from Kauai, Hawaii. Cont Min and Petr 99:202-218

Clague D.A., Frey F.A. (1982) Petrology and trace element geochemistry of the Honolulu Volcanics, Oahu: Implications for the oceanic mantle below Hawaii. J Petr 23:447-504

Clague D.A., Dao-Gong C., Murnane R., Beeson M.H., Lanphere M.A., Dalrymple G.B., Friesen W., and Holcomb R.T. (1982) Age and petrology of the Kalaupapa Basalt, Molokai, Hawaii. Pac Sci 36:411-420

Crandell D.R. (1983) Potential hazards from future volcanic eruptions on the island of Maui, Hawaii. USGS Misc Investigation Series Map I-1442

deVries H. (1958) Variation in concentration of radiocarbon with time and location on earth. Proc Koninkl Ned Akad Wetenschap, B61:94-102

Ghiorso M.S., Sack R.O. (1995) Chemical mass transfer in magmatic processes IV. A revised and internally consistent thermodynamic model for the interpolation and extrapolation of liquid-solid equilibria in magmatic systems at elevated temperatures and pressures. Cont Min and Petr 119: 197-212

Horton K.A. (1977) Geology of the upper southwest rift zone of Haleakala Volcano, Maui, Hawaii. [Unpubl. M.S. thesis]: Honolulu, HI, University of Hawaii at Manoa, 115 p

Kromer B., Becker B. (1993) German Oak and Pine ^{14}C calibration, 7200 BC-9400 BC. Radiocarbon 35: 125-135

Lanphere M.A., Dalrymple G.B. (1980) Age and strontium isotopic composition of the Honolulu Volcanic Series, Oahu, Hawaii. Am Jour Sci 280A:736-751

Linick T.W., Long A., Damon P.E., and Ferguson C.W. (1986) High-precision radiocarbon dating of Bristlecone pine from 6554 to 5350 BC. Radiocarbon 28:943-953

LeBas M.J., Le Maitre R.W., Streckeisen A., and Zanettin B. (1986) A chemical classification of volcanic Rocks based on the total alkali-silica diagram. J Petr 27 (pt 3): 745-750

Lipman P.W., Banks N.G. (1987) A'a flow dynamics: Mauna Loa 1984. US Geol Surv Prof Pap 1350:1527-1568

Macdonald G.A. (1978) Geologic map of the crater section of Haleakala National Park, Maui, Hawaii. US Geol Surv Misc Invest Series:I-1088

Macdonald G.A., Finch R.H. (1950) The June 1950 eruption of Mauna Loa, Part II. Volcano Lett 509:1-6

Macdonald G.A, Katsura T. (1964) Chemical composition of Hawaiian lavas. J Petr 5:82-133

Macdonald G.A., Powers H.A. A further contribution to the petrology of Haleakala Volcano, Hawaii. Geol Soc Am Bull 79:877-888

Macdonald G.A., Abbott A.T., and Cox D.C. (1983) Volcanoes in the Sea: Honolulu, University of Hawaii Press, 517 p

Mark R.K., Moore J.G. (1987) Slopes of the Hawaiian Ridge. US Geol Surv Prof Pap 1350:101-107

Moore J.G. (1987) Subsidence of the Hawaiian Ridge. US Geol Surv Prof Pap 1350:85-100

Moore J.G., Clague D.A., Rubin M., and Bohrson W.A. (1987) Hualalai Volcano: A preliminary summary of geologic, petrologic, and geophysical data. US Geol Surv Prof Pap 1350:571-585

Mullineaux D.R., Peterson D.W., and Crandell D.R. (1987) Volcanic hazards in the Hawaiian Islands. US Geol Surv Prof Pap 1350:599-621

Naughton J.J., Macdonald, G.A., and Greenberg, V.A. (1980) Some additional K-Ar ages of Hawaiian rocks: The Maui volcanic complex of Molokai, Maui, Lanai, and Kahoolawe. J Volcanol Geotherm Res 7, pp. 339-355

Nicholls I.A., Ringwood A.E. (1973) Effect of water on olivine stability in tholeiites and the production of silica-saturated magmas in the island-arc environment. J Geol 81: 285-300

Norrish K., Hutton J.T. (1969) An accurate x-ray spectrographic methods for the analysis of a wide range of geological samples. Geochim Cosmochim Acta 33:431-441

Olsson I.U. (1970) Radiocarbon variations and absolute chronology. Proc Twelfth Nobel Symp, Almqvist and Wiksell, Stockholm, and John Wiley, New York, 652 pp.

Oostdam B.L. (1965) Age of lava flows on Haleakala, Maui, Hawaii: Geol Soc Am Bull 76, pp. 393-394.

Pearson G.W., Stuiver M. (1993) High-precision bidecadal calibration of the radiocarbon time scale 500-2500 BC. Radiocarbon 35:25-33

Pearson G.W., Becker B., and Qua F. (1993) High-precision ^{14}C measurement of German and Irish oaks to show the natural ^{14}C variations from 7890 to 5000 BC. Radiocarbon 35:93-104

Pringle III M. (1997) [39]Ar/[40]Ar ages of Hana Volcanics lavas. Scottish Nuclear Reactor Center, Scotland (Personal communication)

Reber G. (1959) Age of lava flows on Haleakala, Hawaii. Geol Soc Am Bull, 70: 1245-1246

Rowland S.K., Walker G.P.L. (1990) Pahoehoe and a'a in Hawaii: volumetric flow rate controls the lava structure. Bull Volcanol 52:615-628

Sinton J.M., Diller D.E., and Chen C-Y. (1987) Geology and petrological evolution of West Maui Volcano. Ibid 13-30

Stearns H.T. (1940) Geology of the Hawaiian Islands. Haw Div Hydrogr Bull 5:164 pp

Stearns H.T. (1946) Geology of the Hawaiian Islands. Haw Div Hydrogr Bull 8:112 pp

Stearns H.T., Macdonald G.A. (1942) Geology and groundwater resources of the island of Maui, Hawaii. Haw Div Hydrogr Bull 7:344 pp

Stuiver M., Braziunas T.F. (1993) Modeling atmospheric ^{14}C influences and ^{14}C ages of marine samples back to 10,000 BC. Radiocarbon 35:137-189

Stuiver M., Pearson G.W. (1993) High-precision bidecadel calibration of the radiocarbon time scale, AD 1950-500 BC and 2500-6000 BC. Rradiocarbon 35:1-23

Stuiver M., Quay P.D. (1981) Atmospheric ^{14}C changes resulting from fossil fuel CO_2 release and cosmic ray flux variability. Earth Plan Sci Lett 53:349-362

Stuiver M., Reimer P.J. (1993) Extended 14C database and revised CALIB radiocarbon calibration program. Radiocarbon 35:215-230

West H.B., Leeman W.P. (1987) Isotopic evolution of lavas from Haleakala Crater, Hawaii. Earth Planet Sci Lett 84:211-225

Yoder H.S., Jr., Tilley C.E. (1962) Origin of basalt magmas: An experimental study of natural and synthetic rock systems. J Petrol 3: 342-352

DATE DUE

DEC 1 5 1999	